

Escape-Zone-Based Optimal Evasion Guidance Against Multiple Orbital Pursuers

Kunpeng Zhang, Yao Zhang

Beijing Institute of Technology

Heng Shi, Huang Huang

Beijing Institute of Control Engineering

Sifeng Bi

University of Strathclyde

Ji Ye, Hongbo Wang

Beijing Institute of Technology

ABSTRACT The orbital evasion problem is getting increasing attention because of the increase of space maneuvering objects. In this paper, an escape-zone-based optimal orbital evasion guidance law for an evading spacecraft on near circular reference orbit is proposed against multiple pursuing spacecraft with impulsive thrust. The relative reachable domain is introduced first and approximated as an ellipsoid propagating along the nominal trajectory under the short-term assumption. The escape zone for the impulsive evasion problem is presented herein as a geometric description of the set of terminal positions for all the impulsive evasion trajectories that are not threatened by the maneuvers of pursuers at the maneuver moment. A general method is developed next to calculate the defined escape zone through finding the intersection of two relative reachable domain approximate ellipsoids at arbitrary intersection moment. Then, the two-sided optimal strategies for the orbital evasion problem are analyzed according to whether the escape zone exists, based on which the escape value is defined and used as the basis of the proposed orbital evasion guidance scheme. Finally, numerical examples demonstrate the usefulness of the presented method for calculating escape zone and the effectiveness of the proposed evasion guidance scheme against multiple pursuing spacecraft.¹

I. Introduction

As the number of near-Earth space objects increases, there is growing attention to the importance of the orbital evasion problem. The problem of orbital evasion originates from the problem of orbital rendezvous and interception, in which the spacecraft needs to evade other maneuvering or non-maneuvering space objects that may be about to collide through its own control [1].

Early studies on orbital evasion were mostly carried out against non-maneuvering space objects. In these research, the evasion strategies were normally generated by maximizing an optimization index such as the terminal miss distance [2][3] or the collision probability [4]. However, these evasion strategies solved by the one-sided optimization cannot be used against a maneuvering space object, since the possible maneuvers of the space object were not considered in these research.

Taking into account the possible maneuvers of the space objects, the traditional collision avoidance problem will become an orbital pursuit-evasion (OPE) problem. The differential game method [5] with maneuver assumptions for both pursuer and evader is more suitable to deal with this two-sided optimal control problem.

Since the differential game theory [6][7] was put forward, many studies on OPE games have been carried out. Analytical methods, for example the closed-form solution of barrier [8], and numerical methods such as the semi-direct collocation nonlinear programming method [9], the multiple shooting method [10], and the dimension-reduction method [11] are two widely used types of methods for solving an OPE game. Moreover, the nonlinear control for OPE game was realized using the state-dependent Riccati equation method in [12]. Two optimal guidance methods, namely, the Cartesian model and the spherical model, for the long-distance OPE game were proposed in [13]. The PE differential game for satellites with continuous thrust was investigated from the viewpoint of reachable domain in [14]. Many other works have focused on solving the saddle point solution of the game quickly and efficiently [15]-[18], as well as the more complex dynamic environment [19][20] and information structure [21].

It should be noted that all of the research above focused on the two-player OPE games involving one evading spacecraft and one pursuing spacecraft with continuous thrust [22]. Almost few studies have been conducted on the orbital evasion strategy against multiple pursuers. Meanwhile, considering the fact that impulsive thrust is still the main form of spacecraft maneuver nowadays, it is required to investigate the impulsive evasion strategy. Reference [23] conducted research aimed at the two-player impulse OPE game, while the assumption of two-impulse transfers is not suitable for short-distance PE. Overall, there is still a gap in the research concerning the impulsive evasion strategy for the short-distance scenario

¹ 0000-0000 © 2023 IEEE

Authors' addresses: Kunpeng Zhang, Yao Zhang, Ji Ye, and Hongbo Wang are with School of Aerospace Engineering, Beijing Institute of Technology, 100081 Beijing, People's Republic of China, Email: (zhangkunpeng@bit.edu.cn, zhangyao@bit.edu.cn, 3120210094@bit.edu.cn, wanghongbo2021@bit.edu.cn). Heng Shi and Huang Huang are with Beijing Institute of Control Engineering,

100094 Beijing, People's Republic of China, Email:

(767903851@qq.com, hhuang33@gmail.com). Sifeng Bi is with Department of Mechanical & Aerospace Engineering, University of Strathclyde, G1 1XJ Glasgow, United Kingdom of Great Britain and Northern Ireland, Email: (sifeng.bi@strath.ac.uk).
(Corresponding author: Yao Zhang.)

against multiple pursuing spacecraft.

According to the initial relative distance between the pursuing spacecraft and evading spacecraft, the orbital evasion problems can be divided into two scenarios [23]: long-distance evasion scenario and short-distance evasion scenario. In contrast, the short-distance evasion scenario, which is closely related to the relative motion state between the pursuing spacecraft and evading spacecraft, is the final stage of the complete orbital evasion process, and has the characteristics of strong adversarial and high real-time requirements. This paper works on the short-distance orbital evasion problem against multiple pursuers with impulsive thrust. There are two main contributions of this paper. The first contribution of this work is to propose the concept of escape zone for an impulsive orbital evasion problem against multiple pursuers, and present an effective method for calculating the escape zone at any decision moment by introducing the approximate relative reachable domain ellipsoid for orbital impulsive maneuver. Second, a two-sided optimization process based on the calculated escape zone is performed to generate the optimal pursuit-evasion strategies, which provides a possible idea for solving impulsive orbital games.

The rest of this paper is organized as follows. Section II introduces the approximate relative reachable domain, and presents the concept of escape zone in this paper. A method based on the approximate relative reachable domain is proposed in Sec. III to calculate the defined escape zone. In Sec. IV, an escape-zone-based optimal evasion guidance law is proposed based on the escape value defined through the two-sided optimal strategies analysis. Numerical examples are provided in Sec. V, and section VI concludes this paper.

II. Preliminaries

A. Relative Reachable Domain Approximate Ellipsoid

The relative reachable domain (RRD) concept is introduced in this paper to determine the potential relative state reach set of a spacecraft under given maneuverability. Different from the concepts in [24] and [25], a RRD denoted by $D(\mathbf{X}_0, \Delta V_{\max}, \Delta t)$ here is described as the set of all possible relative positions that can be transferred to after time Δt from initial relative state \mathbf{X}_0 under the maximum available velocity increment ΔV_{\max} .

Assuming that the reference orbit is circular, the RRD can be established based on the linearized dynamics, i.e., the CW equations [26], which have been proved sufficiently accurate to model the close range relative motion [25], as

$$\begin{cases} (x - x_c)^2 + (y - y_c)^2 \leq (\kappa_1 + \kappa_2)\Delta V_x^2 + (\kappa_2 + \kappa_3)\Delta V_y^2 \\ \quad + (\kappa_4 + \kappa_5)\Delta V_x\Delta V_y \\ (z - z_c)^2 \leq \kappa_z^2\Delta V_z^2 \end{cases} \quad (1)$$

where

$$\begin{aligned} x_c &= (4 - 3c)x_0 + (s/\omega)\dot{x}_0 + 2[(1 - c)/\omega]\dot{y}_0 \\ y_c &= 6(s - \omega\Delta t)x_0 + y_0 + 2[(c - 1)/\omega]\dot{x}_0 + (4s/\omega - 3\Delta t)\dot{y}_0 \\ z_c &= cz_0 + (s/\omega)\dot{z}_0 \\ \kappa_1 &= s^2/\omega^2, \quad \kappa_2 = (4/\omega^2)(c - 1)^2 \\ \kappa_3 &= (4s/\omega - 3\Delta t)^2, \quad \kappa_4 = (4s/\omega^2)(1 - c) \\ \kappa_5 &= (4/\omega)(c - 1)(-3\Delta t + 4s/\omega), \quad \kappa_z = s/\omega \end{aligned} \quad (2)$$

$$\begin{aligned} \Delta V_x &= \Delta V_{\max} \cos \eta_{\Delta V} \cos \xi_{\Delta V} \\ \Delta V_y &= \Delta V_{\max} \cos \eta_{\Delta V} \sin \xi_{\Delta V}, \quad \Delta V_z = \Delta V_{\max} \sin \eta_{\Delta V} \end{aligned} \quad (3)$$

and $s = \sin(\omega\Delta t)$, $c = \cos(\omega\Delta t)$, ω is the mean angular motion of the reference orbit, $x_0, y_0, z_0, \dot{x}_0, \dot{y}_0$, and \dot{z}_0 are components of the initial relative position vector and relative velocity vector in the reference local-vertical, local-horizontal (LVLH) frame, $\xi_{\Delta V}$ and $\eta_{\Delta V}$ are two angles characterizing the direction of the initial impulse vector in the reference LVLH frame.

Obviously, the envelope of the RRD described by Eq. (1) is exactly the boundary of the time-constrained reachable relative state distribution mentioned in [24] and [25] at given time Δt , without considering the initial position uncertainty. Specifically, the commonality between them is that the fixed-time RRD considered in [24] and [25] will be the same as that in this paper if the initial position uncertainties $\Delta \mathbf{r}$ are set to $\mathbf{0}$ and the velocity increment applied at the decision moment is considered as the initial velocity uncertainties $\Delta \mathbf{v}$. The difference between them is that [24] and [25] focus on solving the accurate inner and outer boundaries of the RRD in any direction within a relative motion time range, while this paper focuses on efficiently solving the approximate envelope of the RRD at any given time for quick analysis of the positional relationship between RRDs for different participants in the OPE games.

When the relative motion time is much smaller than the period of the reference orbit, the envelope of the RRD at time Δt can be approximated as

$$\frac{(x - x_c)^2}{(\kappa_{xy}\Delta V_{\max})^2} + \frac{(y - y_c)^2}{(\kappa_{xy}\Delta V_{\max})^2} + \frac{(z - z_c)^2}{(\kappa_z\Delta V_{\max})^2} = 1 \quad (4)$$

where

$$\kappa_{xy} = \sqrt{\kappa_2 + (\kappa_1 + \kappa_3 + \kappa_4 + \kappa_5)/2} \quad (5)$$

It should be noted that the approximation in Eq. (4) occurs only in the x - y reference plane, not in the z direction. Specifically, the right side of the first formula in Eq. (1) is approximated by $(\kappa_{xy}\Delta V_{\max} \cos \eta_{\Delta V})^2$. Let $F_1(\Delta t)$ and $F_2(\Delta t)$ denote the former and latter expression, respectively. $F_1(0) = F_2(0)$ and $\lim_{t \rightarrow 0} |(F_2 - F_1)/F_1| = 0$ can be proved, which demonstrate the equivalence of F_1 and F_2 at $\Delta t = 0$. Furthermore, a quantitative analysis is given as follows to investigate that this approximation is valid for how small the motion time is.

Suppose that the height of the reference orbit is 35786 km, and that $\Delta V_{\max} = 10$ m/s. For each time Δt taken from 0 s to 7% times the reference orbital period T_r , a total of 1000000 Monte Carlo runs calculating the absolute value of relative error (ARE) of relative reachable distances are performed with different $\xi_{\Delta V} \in [0, 2\pi)$ and $\eta_{\Delta V} \in [-\pi/2, \pi/2]$. The results of the Monte Carlo runs are shown in Fig. 1. As seen in Fig. 1, the mean ARE is less than 3% (considered as the maximum value for an acceptable approximation error) when Δt is less than about 6.665% $T_r = 5741.372$ s. Similarly, the maximum ARE is less than 3% when Δt is less than about 4.797% $T_r = 4132.237$ s. The results for other orbital heights and impulse magnitudes are also analogous to that in Fig. 1, some of which are given in Table 1 and Table 2.

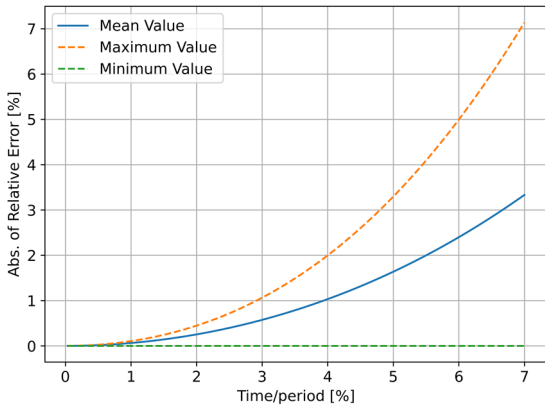


Fig. 1 Results of the Monte Carlo runs.

Table 1 Results for more reference orbital heights

Orbital height (km)	Maximum Δt when mean ARE < 3%	Maximum Δt when maximum ARE < 3%
400	6.665289% T_r	4.797518% T_r
1000	6.665305% T_r	4.797339% T_r
5000	6.665294% T_r	4.797338% T_r
10000	6.665289% T_r	4.797333% T_r
20200	6.665288% T_r	4.797352% T_r
36300	6.665402% T_r	4.797374% T_r

Table 2 Results for more impulse magnitudes

Impulse Magnitude ΔV_{\max} (m/s)	Maximum Δt when mean ARE < 3%	Maximum Δt when maximum ARE < 3%
2	6.665292% T_r	4.797359% T_r
5	6.665329% T_r	4.797409% T_r
8	6.665283% T_r	4.797325% T_r
15	6.665294% T_r	4.797337% T_r
18	6.665318% T_r	4.797273% T_r
20	6.665359% T_r	4.797416% T_r

Accordingly, the following conclusions are obtained about the approximate envelope defined in Eq. (4):

1) The approximate envelope of the RRD at time Δt is an ellipsoid of revolution (termed RRDE) in the reference LVLH frame, which is centered on the nominal relative position at time Δt , with $a = b = \kappa_{xy} \Delta V_{\max}$ and $c = \kappa_z \Delta V_{\max}$ as the major and minor semi axes respectively, as shown in Fig. 2.

2) The error caused by the approximation is acceptable only when Δt is much smaller than T_r (termed short-term assumption). Specifically, Δt needs to be less than about $\tau_1 = 6.665\%T_r$ or $\tau_2 = 4.797\%T_r$, so as to ensure that the mean ARE or maximum ARE is less than 3%, respectively.

3) Under the short-term assumption, a and c both increase monotonically with increasing time Δt .

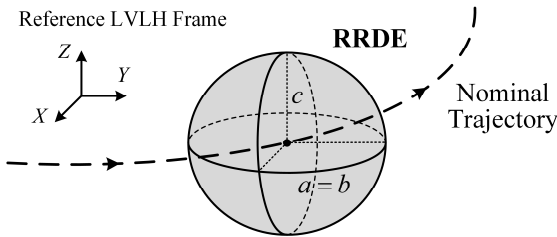


Fig. 2 Approximate ellipsoid of the RRD.

B. Problem Statement and Escape Zone Definition

Consider an orbital evasion problem against N pursuing spacecraft. Each participating spacecraft is controlled by a three-dimensional impulse input at each decision moment, which represents the thrust effect during this decision period. The pursuing spacecraft attempts to satisfy some certain intercept conditions, for example, position matching with the evader. Contrarily, the evader needs to avoid entering this terminal interception range through its own control.

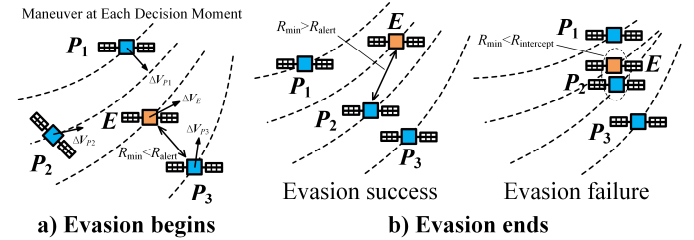
Before continuing, the following assumptions are made:

1) All the participating spacecraft are assumed to move in a two-body gravitational field, without considering any forms of perturbations and real-world noises.

2) The maneuverability of the evader is assumed to be stronger than that of the pursuer to ensure escape is possible [27]. Specifically, two sides of the game are assumed to maneuver at the same time [28]. Meanwhile, the decision periods for the pursuers and evader are the same, but the maximum available velocity increment of the single impulse for the evader is slightly larger than that of the pursuer.

3) The observation information is assumed to be complete, that is, each participating spacecraft can accurately acquire the status of other spacecraft in real time.

As shown in Fig. 3, the evasion process starts from the moment t_0 when the minimum distance R_{\min} between the pursuers and evader is less than a given alert distance R_{alert} , for example, 100 km, and terminates when R_{\min} is less than the minimum valid interception distance $R_{\text{intercept}}$ of pursuers (evasion failure) or when R_{\min} is larger than R_{alert} again (evasion success). Therefore, the entire pursuit-evasion motion can be considered as the close range relative motion.


 Fig. 3 Diagram of the evasion problem (e.g. $N=3$).

For the above orbital evasion problem, a unified time RRD ellipsoid of the evader (termed UTRRDE) at time t_U is proposed first, where t_U is a unified time introduced to unify different RRD ellipsoids for different intersection moments herein. There is no strict constraint on the selection of the unified time t_U as long as it is larger than the decision moment t_0 when the impulse is applied, i.e. the relative motion time ($t_U - t_0$) is positive, to ensure that the geometric parameters a and c of UTRRDE are larger than 0. However, considering the approximation error caused by the RRD ellipsoid, it is suggested to select a unified time less than the maximum valid relative motion time $\tau_1 = 6.665\%T_r$ determined in Sec. IIA to reduce the guidance error.

In this paper, the corresponding point M^{t_U} on the UTRRDE for a point M on the $RRDE_E$ at time t is defined as the terminal relative position point after time t_U on the impulsive relative trajectory (termed the characteristic trajectory), along which the evader can transfer to M after time t .

The corresponding point M_1^{TU} of a point M_1 on the intersection curve I_1 of two RRDEs at time t can be calculated as follows: The velocity increment of the characteristic trajectory for M_1 and M_1^{TU} is computed first by

$$\Delta V_{M_1} = [A_{TU}(t)]^{-1} [x_{M_1} \ y_{M_1} \ z_{M_1}]^T \quad (6)$$

where

$$A_{TU}(t) = \begin{bmatrix} \frac{\sin(\omega t)}{\omega} & \frac{2}{\omega} [1 - \cos(\omega t)] & 0 \\ -\frac{2}{\omega} [1 - \cos(\omega t)] & -3t + \frac{4}{\omega} \sin(\omega t) & 0 \\ 0 & 0 & \frac{\sin(\omega t)}{\omega} \end{bmatrix} \quad (7)$$

represents the state transition matrix from the initial impulse to the relative position at time t in the reference orbital frame, x_{M_1} , y_{M_1} , and z_{M_1} are components of the relative position vector of M_1 in the reference LVLH frame. Then, the corresponding point M_1^{TU} can be obtained by

$$\begin{bmatrix} x_{M_1^{TU}} & y_{M_1^{TU}} & z_{M_1^{TU}} \end{bmatrix}^T = A_{TU}(t_U) \Delta V_{M_1} \quad (8)$$

In this regard, the concept of escape zone (EZ) here proposed for the above evasion problem is defined as follows: Let $\Phi_t^{t_U}$ denote the EZ at decision moment t respect to the unified moment t_U , where $t_U > t$. Define the initial reference orbit with the initial orbit of evader. As shown in Fig. 4, $\Phi_t^{t_U}$ is a combined area on the RRDE at time $(t_U - t)$, and all transfer trajectories that can reach to this area after time $(t_U - t)$ through a single velocity impulse, the magnitude of which is not larger than ΔV_{\max} , can escape the interception of pursuers.

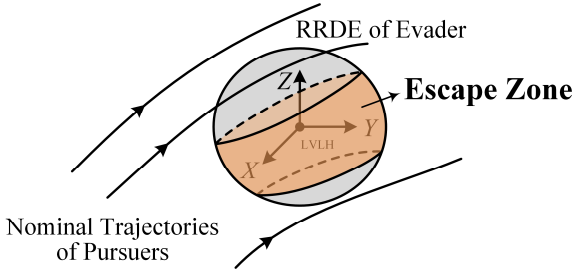


Fig. 4 Definition of the escape zone.

III. Escape Zone Calculation

In this section, a method for finding the intersection of two RRDEs is presented first. The largest threatened area on the RRDE of evader by each pursuing spacecraft is solved then, and the EZ is eventually obtained by successively removing these areas from the entire ellipsoid.

A. Finding Intersection of Two RRDEs

Let the initial time $t_0 = 0$. Define the initial reference orbit with the initial orbit of evader, in which way the center of the RRDE of evader will always be located at the origin of the reference orbital frame. Suppose that the RRDE of pursuer P ($RRDE_P$) intersects that of evader E ($RRDE_E$) at time t , as shown in Fig. 5. The intersection of two RRDEs represented by the red line I_1 in Fig. 5 can be solved as follows.

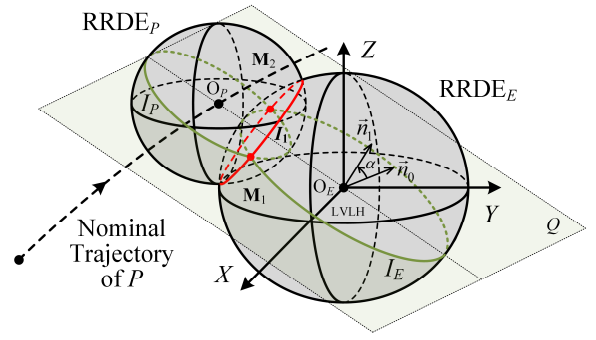


Fig. 5 Intersection of two RRDEs at time t .

Let O_P and O_E denote the center of the $RRDE_P$ and $RRDE_E$, respectively. For the plane Q_0 determined by the line $O_P O_E$ and Z axis of the reference frame, the components of its normal vector \vec{n}_0 in the reference LVLH frame is

$$\mathbf{r}_{n_0} = ([0 \ 0 \ 1]^T)^{\times} \mathbf{r}_{O_P} = ([0 \ 0 \ 1]^T)^{\times} [x_{cP} \ y_{cP} \ z_{cP}]^T \quad (9)$$

where x_{cP} , y_{cP} , and z_{cP} are components of the nominal relative position vector of P at time t in the reference LVLH frame.

The plane Q defined by

$$Q: px + qy + rz = 0 \quad (10)$$

is obtained by rotating Q_0 about the line $O_P O_E$ by angle α . According to the Rodrigues' Rotation Formula [29], the parameters p , q , and r in Eq. (10) can be computed by

$$[p \ q \ r]^T = \mathbf{r}_{n_0} \cos \alpha + \mathbf{r}_{O_P}^{\times} \mathbf{r}_{n_0} \sin \alpha + (\mathbf{r}_{O_P} \cdot \mathbf{r}_{n_0}) \mathbf{r}_{O_P} (1 - \cos \alpha) \quad (11)$$

Let a_P , c_P and a_E , c_E denote the geometric parameters of $RRDE_P$ and $RRDE_E$, respectively. Then, the ellipsoids of P and E can be defined by

$$\begin{aligned} RRDE_P: & \frac{(x - x_{cP})^2}{a_P^2} + \frac{(y - y_{cP})^2}{a_P^2} + \frac{(z - z_{cP})^2}{c_P^2} = 1 \\ RRDE_E: & \frac{x^2}{a_E^2} + \frac{y^2}{a_E^2} + \frac{z^2}{c_E^2} = 1 \end{aligned} \quad (12)$$

The plane Q intersects the $RRDE_P$ and $RRDE_E$ at the curve I_P and I_E , respectively, as shown by the green lines in Fig. 5. Evidently, the intersection curves I_P and I_E must be ellipses or circles [30]. If and only if the plane Q is the equatorial plane of the RRDE, the intersection curve is a circle. Let

$$\lambda_i = \sqrt{(a_i p)^2 + (a_i q)^2 + (c_i r)^2}, \quad (i = P, E) \quad (13)$$

By using the Householder transformation [31], the parametric equation [32] of the intersection curve I_i can be given by

$$\begin{aligned} x_{i1}(\varphi_i) &= \frac{a_i}{\lambda_i (c_i r - \lambda_i)} \{ [\lambda_i (c_i r - \lambda_i) + (a_i p)^2] \cos \varphi_i + a_i^2 p q \sin \varphi_i \} + x_{ci} \\ y_{i1}(\varphi_i) &= \frac{a_i}{\lambda_i (c_i r - \lambda_i)} \{ a_i^2 p q \cos \varphi_i + [\lambda_i (c_i r - \lambda_i) + (a_i q)^2] \sin \varphi_i \} + y_{ci} \\ z_{i1}(\varphi_i) &= \frac{c_i}{\lambda_i} (a_i p \cos \varphi_i + a_i q \sin \varphi_i) + z_{ci} \end{aligned} \quad (14)$$

where $x_{cE} = y_{cE} = z_{cE} = 0$, and $\varphi_i \in [0, 2\pi]$ is the phase parameter of each point on I_i .

Then, two intersection points M_1 and M_2 of I_P and I_E , both of which lie on the intersection curve I_1 of two RRDEs, can be calculated by solving the equations $x_{IP} = x_{IE}$, $y_{IP} = y_{IE}$, and $z_{IP} = z_{IE}$. However, this problem is difficult to solve analytically because of the high nonlinearity in Eq. (14). In this regard, the numerical solution is obtained here, by minimizing the objective function that $F_{I1} = (x_{IP} - x_{IE})^2 + (y_{IP} - y_{IE})^2 + (z_{IP} - z_{IE})^2$.

$-z_{IE})^2$ for design variables $\varphi_p \in [0, 2\pi]$ and $\varphi_E \in [0, 2\pi]$ through the nonlinear optimization method, for example, the Quasi-Newton Method [33].

In order to improve the convergence of the above optimization process, the phases of the intersection points M_1' and M_2' of two circles obtained by the intersection of plane Q and each RRD approximate sphere (RRDS) are used to provide initial guesses for φ_i , as shown in Fig. 6, where the RRDS is a sphere whose center coincides with the center of RRDE and whose radius is equal to a of RRDE. Meanwhile, the Jacobian matrix of the objective function is provided by

$$\mathbf{J}_{I_1} = \begin{bmatrix} \frac{\partial F_{I_1}}{\partial \varphi_E} & \frac{\partial F_{I_1}}{\partial \varphi_P} \end{bmatrix} \quad (15)$$

where

$$\begin{aligned} \frac{\partial F_{I_1}}{\partial \varphi_E} = & \left(\frac{2a_E}{\lambda_E(c_E r - \lambda_E)} \{ [\lambda_E(c_E r - \lambda_E) + (a_E p)^2] \cos \varphi_E \right. \\ & + a_E^2 p q \sin \varphi_E \} - \frac{2a_P}{\lambda_P(c_P r - \lambda_P)} \{ [\lambda_P(c_P r - \lambda_P) + (a_P p)^2] \cos \varphi_P \\ & + a_P^2 p q \sin \varphi_P \} - 2x_{cP} \frac{a_E}{\lambda_E(c_E r - \lambda_E)} \{ a_E^2 p q \cos \varphi_E - [\lambda_E(c_E r \\ & - \lambda_E) + (a_E p)^2] \sin \varphi_E \} + \left(\frac{2a_E}{\lambda_E(c_E r - \lambda_E)} \{ a_E^2 p q \cos \varphi_E \right. \\ & + [\lambda_E(c_E r - \lambda_E) + (a_E q)^2] \sin \varphi_E \} - \frac{2a_P}{\lambda_P(c_P r - \lambda_P)} \{ a_P^2 p q \cos \varphi_P \\ & + [\lambda_P(c_P r - \lambda_P) + (a_P q)^2] \sin \varphi_P \} - 2y_{cP} \frac{a_E}{\lambda_E(c_E r - \lambda_E)} \{ [\lambda_E(c_E r \\ & - \lambda_E) + (a_E q)^2] \cos \varphi_E - a_E^2 p q \sin \varphi_E \} + \left[\frac{2c_E}{\lambda_E} (a_E p \cos \varphi_E \right. \\ & + a_E q \sin \varphi_E) - \frac{2c_P}{\lambda_P} (a_P p \cos \varphi_P + a_P q \sin \varphi_P) \\ & \left. - 2z_{cP} \right] \frac{c_E}{\lambda_E} (a_E q \cos \varphi_E - a_E p \sin \varphi_E) \end{aligned} \quad (16)$$

and

$$\begin{aligned} \frac{\partial F_{I_1}}{\partial \varphi_P} = & \left(\frac{2a_P}{\lambda_P(c_P r - \lambda_P)} \{ [\lambda_P(c_P r - \lambda_P) + (a_P p)^2] \cos \varphi_P \right. \\ & + a_P^2 p q \sin \varphi_P \} + 2x_{cP} \frac{a_E}{\lambda_E(c_E r - \lambda_E)} \{ [\lambda_E(c_E r - \lambda_E) + (a_E p)^2] \\ & \cdot \cos \varphi_E + a_E^2 p q \sin \varphi_E \} - \frac{a_P}{\lambda_P(c_P r - \lambda_P)} \{ a_P^2 p q \cos \varphi_P - [\lambda_P(c_P r \\ & - \lambda_P) + (a_P p)^2] \sin \varphi_P \} + \left(\frac{2a_P}{\lambda_P(c_P r - \lambda_P)} \{ a_P^2 p q \cos \varphi_P + [\lambda_P(c_P r \\ & - \lambda_P) + (a_P q)^2] \sin \varphi_P \} + 2y_{cP} \frac{a_E}{\lambda_E(c_E r - \lambda_E)} \{ a_E^2 p q \cos \varphi_E \right. \\ & + [\lambda_E(c_E r - \lambda_E) + (a_E q)^2] \sin \varphi_E \} - \frac{a_P}{\lambda_P(c_P r - \lambda_P)} \{ [\lambda_P(c_P r - \lambda_P) \\ & + (a_P q)^2] \cos \varphi_P - a_P^2 p q \sin \varphi_P \} + \frac{c_P}{\lambda_P} \left[\frac{2c_P}{\lambda_P} (a_P p \cos \varphi_P \right. \\ & + a_P q \sin \varphi_P) + 2z_{cP} - \frac{c_E}{\lambda_E} (a_E p \cos \varphi_E \\ & \left. + a_E q \sin \varphi_E) \right] (a_P q \cos \varphi_P - a_P p \sin \varphi_P) \end{aligned} \quad (17)$$

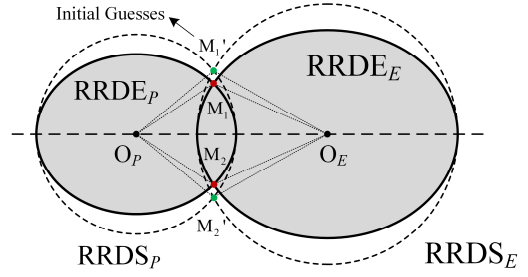


Fig. 6 Initial guesses provided by intersections of RRDSs.

In this manner, the intersection curve I_1 of the RRDE_P and RRDE_E at time t can be obtained ultimately by calculating the intersection points of I_P and I_E for every rotation angle α from 0 to π . Considering that the three main axes of RRDE_P and those of RRDE_E are parallel respectively, the symmetry can be utilized here to calculate the intersection points of I_P and I_E for α from $\pi/2$ to π by directly using the results for α from 0 to $\pi/2$ according to

$$\begin{cases} x_4 = x_3 + 2y_{cP}(-y_{cP}x_3 + x_{cP}y_3) / (y_{cP}^2 + x_{cP}^2) \\ y_4 = y_3 - 2x_{cP}(-y_{cP}x_3 + x_{cP}y_3) / (y_{cP}^2 + x_{cP}^2) \\ z_4 = z_3 \end{cases} \quad (18)$$

where $M_4(x_4, y_4, z_4)$ is the symmetrical intersection point for α from $\pi/2$ to π of the intersection point $M_3(x_3, y_3, z_3)$ for α from 0 to $\pi/2$. Therefore, the computational effort can be eventually reduced by only calculating the intersection points of I_P and I_E for α from 0 to $\pi/2$.

Because the calculated intersection curves I_1 for different intersection times are located on different RRDEs, it is hard to compare them quantitatively. To solve this problem, the unified time RRD ellipsoid presented in Sec. IIB is introduced here. Through Eqs. (6) to (8), the intersection I_1 for any intersection time can be projected onto the same UTRRDE to obtain the corresponding curve I_2 , as shown in Fig. 7.

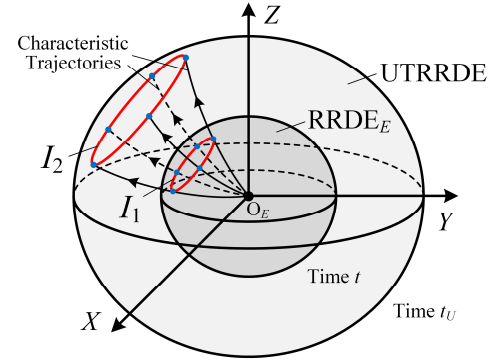


Fig. 7 Curve I_2 corresponding to intersection I_1 .

B. Solving the Largest Coverage on UTRRDE

To solve the largest coverage on the UTRRDE swept by the pursuer P during the entire relative motion process, the RRDE of P and the RRDE of the evader E are propagated along the time axis. Firstly, the positional relationship between two RRDEs at the given time t can be judged as follows:

Rewrite Eq. (12) into the following quadratic equations:

$$\begin{aligned} \text{RRDE}_E : \mathcal{Q}_E(\mathbf{X}) &= \mathbf{X}^T \mathbf{A}_E \mathbf{X} + \mathbf{C}_E = 0 \\ \text{RRDE}_P : \mathcal{Q}_P(\mathbf{X}) &= \mathbf{X}^T \mathbf{A}_P \mathbf{X} + \mathbf{B}_P^T \mathbf{X} + \mathbf{C}_P = 0 \end{aligned} \quad (19)$$

where

$$\mathbf{X} = \begin{bmatrix} x \\ y \\ z \end{bmatrix}, \mathbf{A}_E = \begin{bmatrix} c_E^2 & 0 & 0 \\ 0 & c_E^2 & 0 \\ 0 & 0 & a_E^2 \end{bmatrix}, C_E = -a_E^2 c_E^2$$

$$\mathbf{A}_P = \begin{bmatrix} c_P^2 & 0 & 0 \\ 0 & c_P^2 & 0 \\ 0 & 0 & a_P^2 \end{bmatrix}, \mathbf{B}_P = \begin{bmatrix} -2c_P^2 x_{cP} \\ -2c_P^2 y_{cP} \\ -2a_P^2 z_{cP} \end{bmatrix} \quad (20)$$

$$C_P = c_P^2 x_{cP}^2 + c_P^2 y_{cP}^2 + a_P^2 z_{cP}^2 - a_P^2 c_P^2$$

Since \mathbf{A}_E and \mathbf{A}_P are positive definite, $Q_i(\mathbf{X}) < 0$, ($i = P, E$) defines the inside of the RRDE $_i$, and $Q_i(\mathbf{X}) > 0$ corresponds to the outside.

Generally, $Q_E(\mathbf{X}) = \lambda$ define all level curve ellipsoids [34] of RRDE $_E$, where the minimum (negative) value of λ and $\lambda = 0$ define the O_E and the RRDE $_E$, respectively. The minimum level value λ_0 and maximum level value λ_1 of the level curve ellipsoids that intersect the RRDE $_P$ can be calculated by minimizing $Q_E(\mathbf{X})$ subject to the constraint $Q_P(\mathbf{X}) = 0$, which can be solved by the method of Lagrange multipliers [35].

Define the Lagrange function as

$$F(\mathbf{X}, \varepsilon) = Q_E(\mathbf{X}) + \varepsilon Q_P(\mathbf{X}) \quad (21)$$

where ε is the introduced Lagrange multiplier. Differentiating Eq. (21) yields

$$\nabla F = \nabla Q_E + \varepsilon \nabla Q_P \quad (22)$$

$$\partial F / \partial \varepsilon = Q_P \quad (23)$$

where the gradient ∇ represents the derivatives in \mathbf{X} .

Setting Eq. (22) equal to zero yields

$$\nabla Q_E + \varepsilon \nabla Q_P = 2(\mathbf{A}_E + \varepsilon \mathbf{A}_P)\mathbf{X} + \varepsilon \mathbf{B}_P = \mathbf{0} \quad (24)$$

Formally solving for \mathbf{X} yields

$$\mathbf{X} = -\frac{\varepsilon}{2}(\mathbf{A}_E + \varepsilon \mathbf{A}_P)^{-1} \mathbf{B}_P = \frac{\mathbf{Y}(\varepsilon)}{\delta(\varepsilon)} \quad (25)$$

where $\delta(\varepsilon) = \det(\mathbf{A}_E + \varepsilon \mathbf{A}_P)$ is a cubic polynomial in ε , and $\mathbf{Y}(\varepsilon)$ is a column vector that has components cubic in ε .

Setting Eq. (23) equal to zero and replacing \mathbf{X} with Eq. (25) yields

$$\mathbf{Y}(\varepsilon)^T \mathbf{A}_P \mathbf{Y}(\varepsilon) + \delta(\varepsilon) \mathbf{B}_P^T \mathbf{Y}(\varepsilon) + \delta(\varepsilon)^2 C_P = 0 \quad (26)$$

which is a degree six polynomial in ε . The \mathbf{X} can be computed by substituting the computed roots [36] of Eq. (26) into Eq. (25), and the corresponding value of $Q_E(\mathbf{X})$ can be calculated by Eq. (19). The minimum and maximum values of the calculated $Q_E(\mathbf{X})$ are exactly λ_0 and λ_1 , respectively.

The positional relationship between two RRDEs at time t can be decided by comparing λ_0 and λ_1 with 0: If $\lambda_0 > 0$, two RRDEs are separated. If $\lambda_0 < 0$ and $\lambda_1 > 0$, two RRDEs intersect. If $\lambda_1 < 0$, the RRDE $_P$ is contained in the RRDE $_E$.

Then, three cases about the types of the nominal relative trajectory of P are discussed according to the positional relationships between two RRDEs along the time axis:

1) Case 1, *separation*. If $\lambda_0 > 0$ holds for any time t , then the largest coverage does not exist, since the two RRDEs do not intersect at any time (see Fig. 8a).

2) Case 2, *intersection*. If $\lambda_1 > 0$ holds for any time t , and there exist time t such that $\lambda_0 < 0$, then the two RRDEs intersect in a period of time between t_{ex1} and t_{ex2} , where t_{ex1} and t_{ex2}

represent the first and the second externally tangent time of two RRDEs, respectively (see Fig. 8b). Therefore, the largest coverage is a continuous area on the UTRRDE swept by P during the time interval (t_{ex1}, t_{ex2}) .

3) Case 3, *contained*. If there exist time t such that $\lambda_1 < 0$, then the two RRDEs intersect in two time intervals, between which the RRDE $_P$ is totally contained in the RRDE $_E$, as shown in Fig. 8c. Therefore, the largest coverage contains two separate areas on the UTRRDE successively swept by P during the time interval (t_{ex1}, t_{in1}) and (t_{in2}, t_{ex2}) .

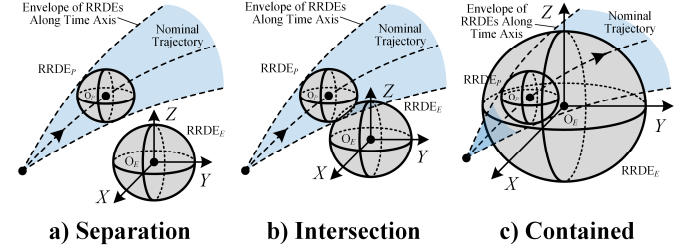


Fig. 8 Three cases of nominal trajectory of pursuer.

Let T_P denote the largest coverage of P . As mentioned, for the *separation* case, $T_P = \emptyset$. For the *intersection* case, T_P is the union of all the areas enclosed by the intersection curve I_2 during the time interval (t_{ex1}, t_{ex2}) , as shown in Fig. 9a. Similarly, for the *contained* case, T_P is the union of all the areas enclosed by the intersection curve I_2 during the time interval (t_{ex1}, t_{in1}) and (t_{in2}, t_{ex2}) , as shown in Fig. 9b.

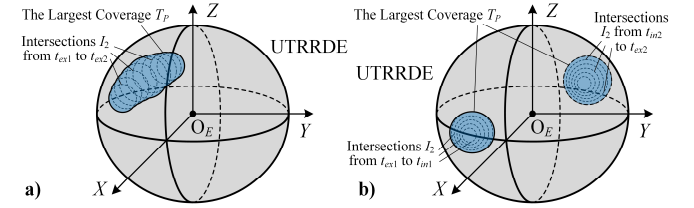


Fig. 9 T_P for the *intersection* and *contained* case.

Considering the infinity of numbers of the rotation angle α around the line $O_P O_E$ and the intersection moment t on the time axis, an ellipsoidal polygon with finite vertices, which all lie on the intersection curve I_2 , is used to replace I_2 , and a time step is selected for discrete calculations along the time axis. Specifically, the larger the number of polygon vertices and the smaller the time step, the higher the solution accuracy but the higher the computational burden. Under this approximation, the union of two intersection curve areas at different intersection time can be calculated by judging the inclusion relationships of the vertices of two ellipsoidal polygons [37].

In this way, T_P of each pursuing spacecraft is recorded as a data table, which takes the intersection time t as the data index, and the geodetic coordinates of all vertices of the approximate polygon of the intersection curve I_2 at time t as the data value, and is stored in a database for all the pursuers. The boundary of T_P is recorded as a series of vertices associate with the intersection times.

Eventually, the escape zone can be obtained by considering the threats of all the pursuing spacecraft. Let T_{Pi} , ($i = 1, 2, \dots, N$) denote the largest coverage of pursuing spacecraft P_i solved at the decision moment t . For $R_{\text{intercept}} = 0$, the escape zone $\Phi_i^{t_0}$

(see Fig. 10) can be calculated ultimately by removing all these largest coverage from the entire unified time ellipsoid

$$\Phi_t^{t_U} \triangleq \Phi_0 - (T_{P_1} \cup T_{P_2} \cup \dots \cup T_{P_N}) \quad (27)$$

where Φ_0 is the entire UTRRDE at the unified time t_U .

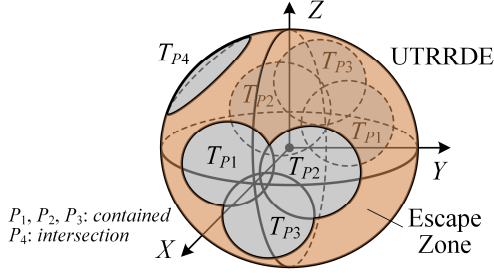


Fig. 10 Diagram of the calculated EZ (e.g. $N = 4$).

IV. Optimal Evasion Guidance Law

In this section, the analysis of the two-sided optimal strategies for this orbital evasion problem is presented first, and the concept of the escape value is proposed next. Finally, a proposed escape-value-optimal guidance law is given to avoid interception by multiple pursuing spacecraft.

A. Two-Sided Optimal Strategies Analysis

In order to ensure the security of the evasion trajectory, the optimal interception strategy of the pursuers for a given evasion trajectory needs to be analyzed.

Before discussion, the concepts of the evasion impulse and the pursuit impulse are clarified first. An evasion impulse here denoted by $\Delta V_E[r_d, t_U]$ represents the impulse of the characteristic trajectory with the terminal position r_d on the UTRRDE. A pursuit impulse here denoted by $\Delta V_{P_i}[r_d, t]$ represents the impulse of the relative transfer trajectory of P_i that can make P_i intercept the evader after time t , which moves along the characteristic trajectory with the terminal position r_d on the UTRRDE. According to Sec. III, the terminal position r_d is exactly located on the intersection curve I_2 of the intersection time t on the UTRRDE.

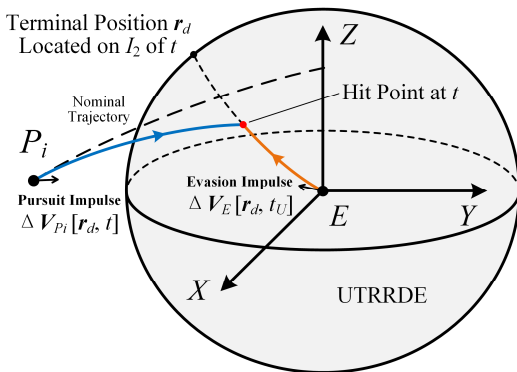


Fig. 11 The evasion impulse and the pursuit impulse.

Two cases about the two-sided optimal strategies at decision moment t are discussed as follows:

1) If $\Phi_t^{t_U} \neq \emptyset$, i.e., the calculated EZ is not empty, then any evasion impulse $\Delta V_E[r_d, t_U]$ satisfying that $r_d \in \Phi_t^{t_U}$ leads to a successful evasion, which means that the pursuers cannot intercept the evading spacecraft with above evasion impulse in

a limited time, no matter what strategy they adopt.

In this case, the pursuers will attempt to minimize the miss distances with the maneuvered evader intuitively. On the contrary, the evading spacecraft needs to maximize the minimum miss distance of all pursuers among all the successful evasion trajectories.

The miss distance M_{P_i} is defined as the minimum distance between the maneuvered pursuer P_i and the maneuvered evader E along the time axis, which can be calculated by $M_{P_i} = \min\{|r_{P_i}(t) - r_E(t)| | t \in [0, \tau]\}$ where $r_{P_i}(t)$ and $r_E(t)$ represent the relative position vector of the maneuvered pursuer P_i and the maneuvered evader E at time t in the reference LVLH frame, respectively. Obviously, the optimal strategy of P_i is to adopt the maneuver impulse that can minimize M_{P_i} . Actually, according to the definition of the largest coverage on the UTRRDE, the minimum miss distance must fall on the situation in which the terminal position of the characteristic trajectory is located on the largest coverage T_{P_i} , since T_{P_i} stands for the boundary of the maximum available velocity increment of P_i . Therefore, the optimal pursuit impulse $\Delta V_{P_i}[r_{d2}, t]$ can be solved by searching r_{d2} and t on T_{P_i} to minimize the miss distance M_{P_i} , which can be represented as an optimization problem as follows:

$$\begin{cases} \min_{r_{d2}} M_{P_i}(\Delta V_{P_i}[r_{d2}, t(r_{d2})], \Delta V_E) \\ \text{s.t. } r_{d2} \in T_{P_i} \end{cases}, \quad (i = 1, 2, \dots, N) \quad (28)$$

The minimum miss distance of all pursuers is finally obtained by $M_{\min} = \min\{M_{P_1}, M_{P_2}, \dots, M_{P_N}\}$. As mentioned, the optimal evasion impulse $\Delta V_E[r_{d1}, t_U]$ can be obtained by searching r_{d1} on the EZ to maximize M_{\min} , which can be represented as

$$\min_{r_{d1}} J_1 = -M_{\min}(\Delta V_{P_i}^*, \Delta V_E[r_{d1}, t_U]) \quad \text{s.t. } r_{d1} \in \Phi_t^{t_U} \quad (29)$$

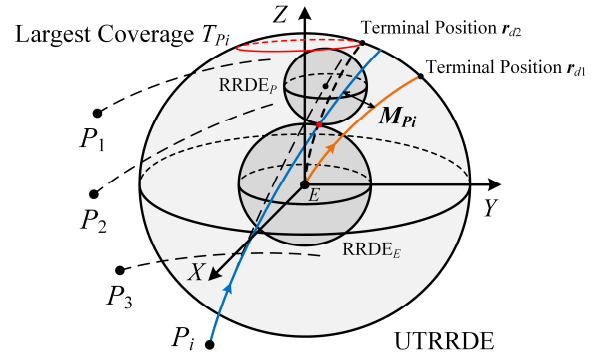


Fig. 12 The optimal strategy of P_i when $EZ \neq \emptyset$.

2) If $\Phi_t^{t_U} = \emptyset$, i.e., the EZ does not exist because the UTRRDE has been completely covered by the threat areas of all pursuers, then the pursuers can always find an appropriate strategy to intercept the evader, no matter what maneuver impulse the evader adopts.

In this case, the pursuers will attempt to minimize the interception time for each given evasion impulse while the evading spacecraft attempts to maximize the minimum time to be intercepted among all the possible evasion trajectories.

With the help of the established database in Sec. III, the minimum time $t_{P_i}^{\min}$ to be intercepted by P_i for a given evasion

trajectory pointing to a certain terminal position \mathbf{r}_{d2} on the UTRRDE can be computed by searching in the database for the minimum intersection time satisfying that the terminal position \mathbf{r}_{d2} is inside the area enclosed by intersection curve I_2 at this intersection time. Then, the optimal impulse of P_i can be determined as $\Delta V_{P_i}[\mathbf{r}_{d2}, t_{P_i}^{\min}]$.

Let t_p^{\min} denote the minimum time among all the valid $t_{P_i}^{\min}$. The optimal evasion impulse $\Delta V_E[\mathbf{r}_{d1}, t_U]$ can be obtained by searching \mathbf{r}_{d1} on Φ_0 to maximize t_p^{\min} , which can be represented as

$$\min_{\mathbf{r}_{d1}} J_2 = -t_p^{\min}(\Delta V_{P_i}^*, \Delta V_E[\mathbf{r}_{d1}, t_U]) \quad \text{s.t. } \mathbf{r}_{d1} \in \Phi_0 \quad (30)$$

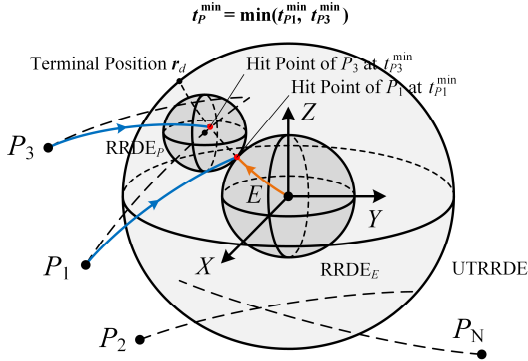


Fig. 13 The optimal strategy of P_i when $EZ = \emptyset$.

B. Escape-Value-Optimal Guidance Law

According to the two-sided optimal strategies, the escape value (EV) is defined here as a scalar describing the effect to escape of an evasion trajectory pointing to the terminal position \mathbf{r}_d on the UTRRDE, which can be computed by

$$V_t^{t_U}(\mathbf{r}_d) \triangleq \begin{cases} -t_p^{\min} / T_{SI} & , \Phi_t^{t_U} = \emptyset \\ -M_{\min} / L_{SI} & , \Phi_t^{t_U} \neq \emptyset \end{cases} \quad (31)$$

where t_p^{\min} is the minimum time to be intercepted of the evader for the given evasion impulse $\Delta V_E[\mathbf{r}_d, t_U]$ when the EZ is empty, T_{SI} is the dimension of time, M_{\min} is the minimum miss distance of all pursuers for the given evasion impulse $\Delta V_E[\mathbf{r}_d, t_U]$ when the EZ is not empty, and L_{SI} is the dimension of distance.

The escape value described previously can be used as the basis for a closed-loop evasion guidance scheme for an evading spacecraft against multiple pursuing spacecraft.

In this scheme, at each decision moment of the evader, the evasion impulse is determined to obtain the largest escape value, which generally implies the greatest evasion possibility. Corresponding to two different cases in the EV calculation, when the EZ exists, the optimal evasion impulse is desired to achieve the largest minimum miss distance of all pursuers. Additionally, when the EZ does not exist, the evasion impulse is still optimized for acquiring the maximum time to be intercepted by the pursuers, which means that every nonoptimal maneuver of the pursuing spacecraft will result in the increase of the interception time and may eventually lead to successful evasion. Such a guidance scheme could be implemented as follows:

- 1) Obtain the current relative states of all N pursuers.
- 2) For the pursuing spacecraft P_i , propagate the nominal

relative motion from the current state to time $T_i/2$ using the nonlinear relative dynamic model [38], which is a fairly sufficient choice to ensure that all externally and internally tangent moments of two RRDEs can be taken into account.

3) Choose a small time step t_s for the RRDE propagation. Calculate λ_0, λ_1 and judge the positional relationship between the $RRDE_{P_i}$ and $RRDE_E$ along the nominal trajectory by Eqs. (19) to (26). Determine the type (*separation, intersection or contained*) of the nominal trajectory for P_i as in Fig. 8, and record the time t_{ex1} and t_{ex2} for the *intersection* case or time $t_{ex1}, t_{in1}, t_{in2}$ and t_{ex2} for the *contained* case.

4) For the *separation* case, let the largest coverage T_{P_i} be empty, and skip to step 7.

5) For the *intersection* or *contained* case, calculate all the intersection curves I_1 of the $RRDE_{P_i}$ and $RRDE_E$ from 0 to τ_1 with time step t_s using the method in Sec. IIIA, and project them onto the UTRRDE through Eqs. (6) to (8) to obtain the corresponding curves I_2 . Save all the curves I_2 into the database for P_i .

6) Calculate the union of all I_2 to obtain T_{P_i} .

7) Repeat the procedure from steps 2 to 6 until the largest coverage of all pursuers have been calculated.

8) Calculate the EZ through Eq. (27).

9) Determine the optimal evasion maneuver by searching \mathbf{r}_d on the EZ (if the EZ is not empty) or on Φ_0 (if the EZ is empty) to minimize the escape value computed by using Eq. (31).

10) This procedure, given by the preceding steps, is continued until the terminal conditions of the evasion process are satisfied. If R_{\min} is larger than R_{alert} , then successful evasion has been attained.

It should be noted that this guidance scheme provides a conservative evasion strategy for the evading spacecraft, in which all the pursuing spacecraft are considered “smart” enough, i.e., will adopt the optimal pursuit strategy. In other words, the provided evasion strategy is a greedy and locally optimal solution rather than the global optimal solution for the entire game with more than one round. However, thanks to the calculated escape zone, this local optimal evasion strategy can be quite concise, fast, and effective. In addition, considering the uncertain antagonism of the pursuers, it is extremely difficult to accurately determine the total number of rounds of the entire game when the strategies of pursuers are unknown, while the guidance scheme could guarantee the basic proceeds of the evading spacecraft in the real-time games.

V. Numerical Examples

In this section, the effectiveness of the proposed evasion guidance scheme is verified by a numerical simulation of an orbital evasion scenario against several pursuing spacecraft.

An evading spacecraft E and four pursuing spacecraft P_1, P_2, P_3, P_4 are included in this orbital evasion scenario, which starts from the initial time $t_0 = 0$ s when the minimum distance R_{\min} between the pursuers and evader is less than the given alert distance $R_{\text{alert}} = 100$ km of evader. The orbital elements at t_0 , including semimajor axis a_0 , eccentricity e_0 , inclination i_0 , right ascension of ascending node Ω_0 , argument of perigee ω_0 , and mean anomaly M_0 , are shown in Table 3.

Table 3 Initial orbital elements of spacecraft

Orbital elements	Evader E	Pursuer P_1	Pursuer P_2	Pursuer P_3	Pursuer P_4
a_0 (km)	42164.1	42792.8	42625.7	42836.2	41518.5
e_0	0.00010	0.01466	0.01218	0.01579	0.01545
i_0 (rad)	0.17453	0.17178	0.17110	0.17791	0.17625
Ω_0 (rad)	1.04720	1.03901	1.03668	1.05799	1.05273
ω_0 (rad)	0.17453	0.65025	0.10889	0.54471	3.65425
M_0 (rad)	0.02780	5.85412	0.09934	5.93882	2.81847

The parameters of mass and maneuverability of the spacecraft are given in Table 4. As mentioned in Sec. IIB, the minimum time interval ΔT_d between two impulses of pursuers and that of the evader are set to be equal, and the maximum available velocity increment 2.4 m/s for each impulse of the evader is set to be larger than that 2 m/s of the pursuer, which conforms to the assumption presented in Sec. IIB that the maximum available velocity increment of the single impulse for the evader is slightly larger than that of the pursuer.

Table 4 Mass and maneuverability parameters of spacecraft

Parameters	Pursuing spacecraft	Evading spacecraft
Mass (kg)	300	500
Maximum thrust (N)	20	40
Minimum time interval between two impulses (s)	300	300
Maximum thrust time of each impulse (s)	30	30
Maximum available velocity increment of each impulse (m/s)	2	2.4

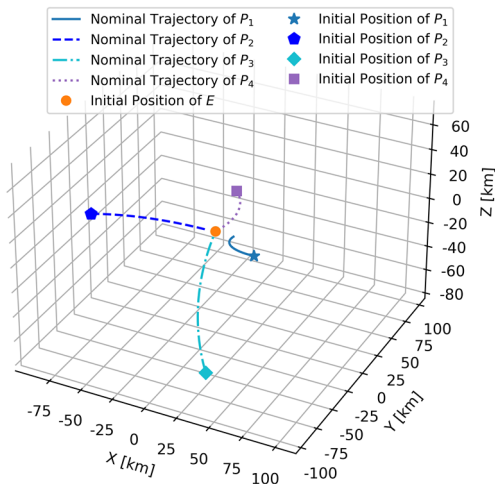


Fig. 14 Initial nominal trajectories of pursuers.

Define the initial reference orbit with the initial orbit of evader. The initial nominal trajectories of pursuers in the reference LVLH frame are portrayed in Fig. 14 according to

Table 3. Suppose that the minimum valid interception distance of pursuers $R_{\text{intercept}} = 1$ km. Then, the initial interception time along the nominal trajectory can be computed as about 4296.284 s for P_3 and 4295.958 s for P_4 , which indicates the necessity of evasion for E .

Two cases of different pursuing strategies are considered: case 1) the optimal pursuing strategy described in Sec. IVA, and case 2) the minimum zero effort miss interception strategy solved by the differential evolution algorithm [39] at each decision moment with the constraint of the maximum available velocity increment $\Delta V_{\text{max}P}$ for each impulse.

The evading spacecraft is guided through the proposed guidance scheme in both cases. All the spacecraft are simulated to move in a two-body gravitational field in the numerical examples. The results and analysis of the numerical examples are presented as follows.

For case 1, the evasion trajectory of evader and the pursuit trajectories of pursuers in reference frame are portrayed in Fig. 15. Projections of these transfer trajectories on the X-Y plane, X-Z plane, and Y-Z plane of the reference LVLH frame are shown in Fig. 16, Fig. 17, and Fig. 18, respectively. Figure 19 portrays the time history of the distance between each pursuing spacecraft and the evading spacecraft. As shown in the figures, the evading spacecraft guided through the proposed scheme successfully escape from all the pursuing spacecraft at 15715.374 s, at which R_{min} is larger than R_{alert} again.

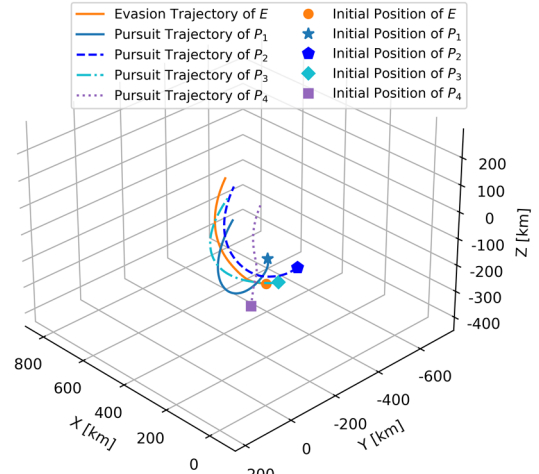


Fig. 15 The evasion and pursuit trajectories in case 1.

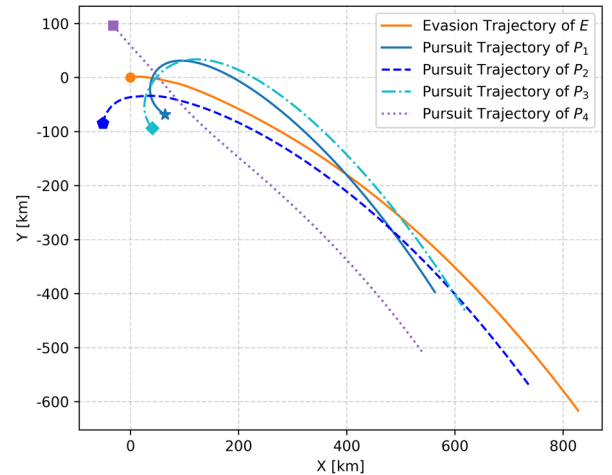


Fig. 16 The X-Y projection of transfer trajectories in case 1.

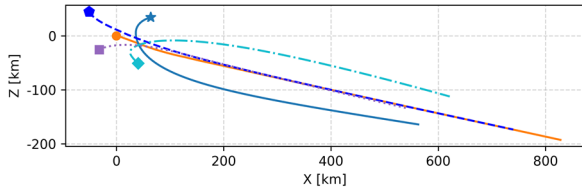


Fig. 17 The X-Z projection of transfer trajectories in case 1.

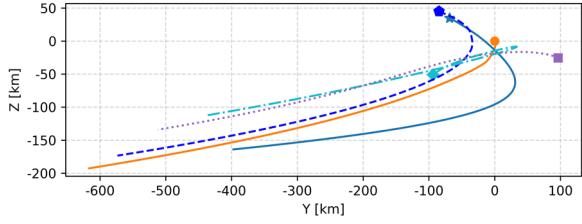
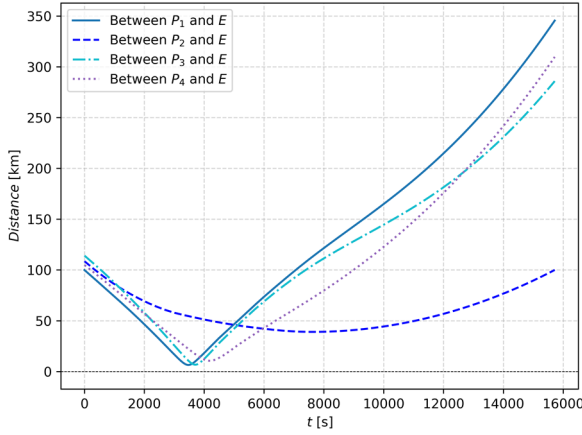


Fig. 18 The Y-Z projection of transfer trajectories in case 1.


 Fig. 19 Distance history between each P and E in case 1.

It is shown in these figures that the entire evasion process can be approximately considered as two stages separated at about 6000 s in case 1. In the first stage, the evading spacecraft attempted to break through the encirclement of the pursuing spacecraft, after which the evader focused on keeping away from all the pursuers through its stronger maneuverability in the second stage. The relative position history shown in Fig. 20 and the pursuit-evasion velocity increment history in the inertial frame shown in Fig. 21 also confirm this ratiocination. The detailed transfer trajectories within 6000 s are portrayed in Fig. 22, where the dashed lines denote the initial nominal trajectories of the pursuers.

To demonstrate the effectiveness of the proposed method for EZ calculation, the results of EZ calculation for the initial time t_0 are provided here. Set the unified time t_U to 4200 s. By using Eqs. (19) to (26), the intersection time intervals of the RRDEs along the nominal trajectories from t_0 are computed as $(t_{ex1}, t_{ex2}) = (3608.974 \text{ s}, 4721.429 \text{ s})$ for P_1 , $(t_{ex1}, t_{ex2}) = (3816.740 \text{ s}, 4859.952 \text{ s})$ for P_2 , $(t_{ex1}, t_{in1}) = (3690.253 \text{ s}, 4235.512 \text{ s})$, $(t_{in2}, t_{ex2}) = (4366.436 \text{ s}, 5166.783 \text{ s})$ for P_3 , and $(t_{ex1}, t_{in1}) = (3644.064 \text{ s}, 4230.013 \text{ s})$, $(t_{in2}, t_{ex2}) = (4372.348 \text{ s}, 5261.372 \text{ s})$ for P_4 . According to Sec. IIIB, the types of the nominal relative trajectory of P_1 , P_2 , P_3 , and P_4 at t_0 can be judged as *intersection*, *intersection*, *contained*, and *contained*, respectively.

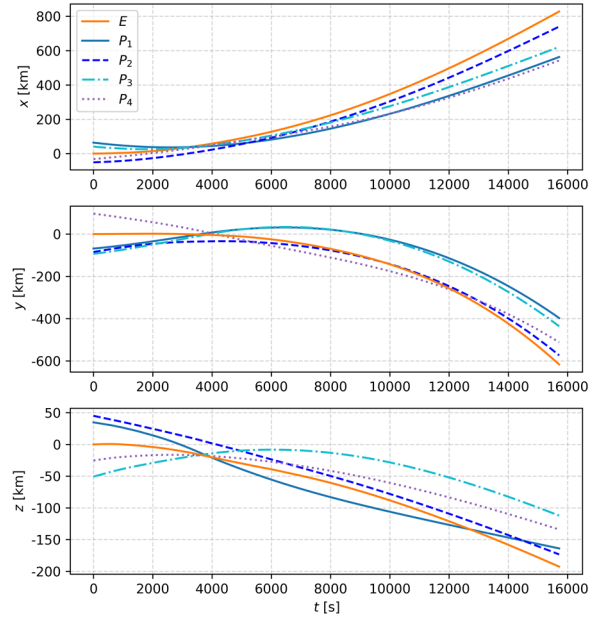


Fig. 20 The relative position history in case 1.

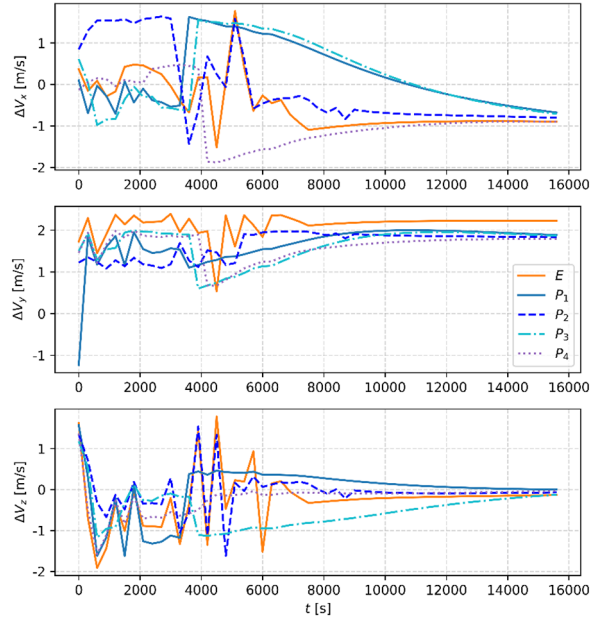


Fig. 21 Pursuit-evasion velocity increment history in case 1.

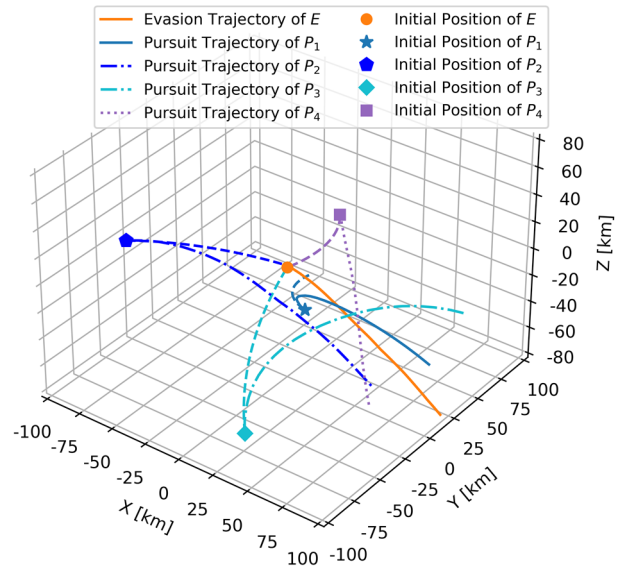
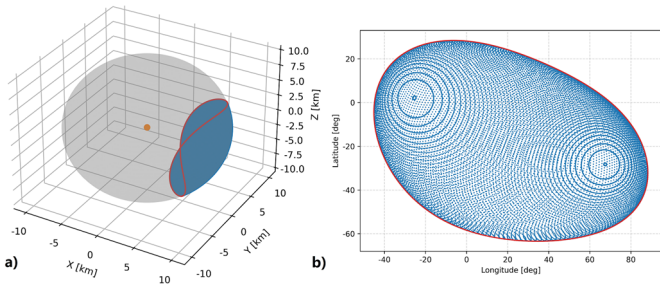
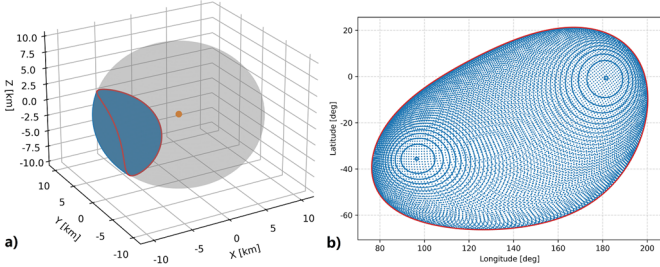
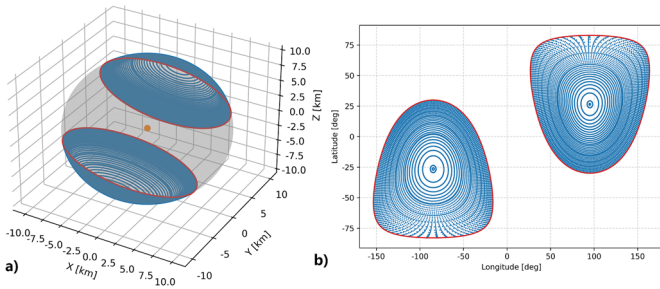
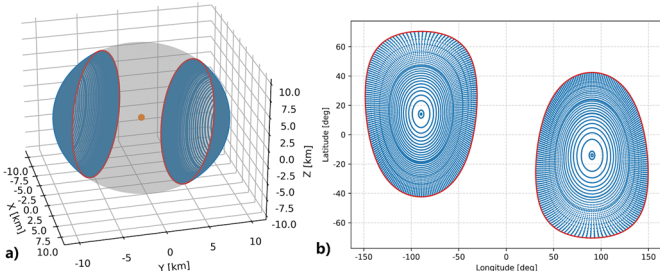
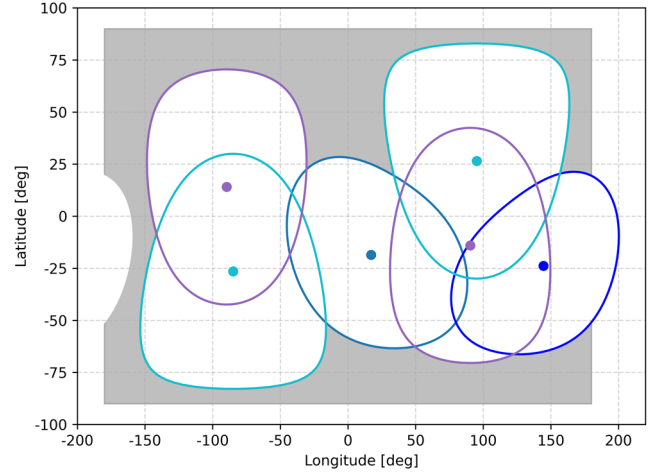


Fig. 22 Detailed trajectories within 6000 s in case 1.

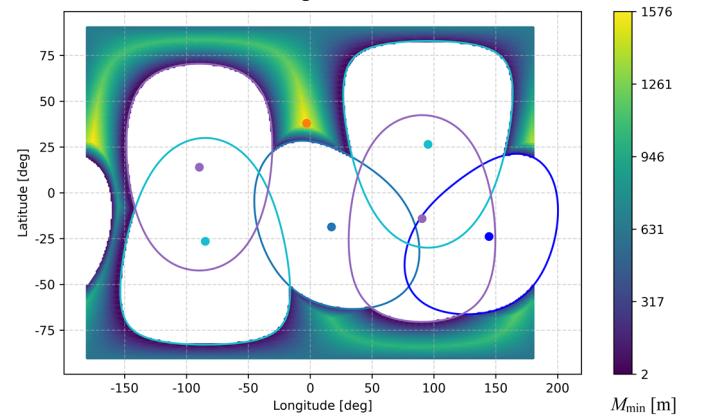

 Fig. 23 Calculated I_2 and TP_1 for P_1 of *intersection* type at t_0 .

 Fig. 24 Calculated I_2 and TP_2 for P_2 of *intersection* type at t_0 .

 Fig. 25 Calculated I_2 and TP_3 for P_3 of *contained* type at t_0 .

 Fig. 26 Calculated I_2 and TP_4 for P_4 of *contained* type at t_0 .

All the intersections I_2 during the intersection time intervals and the largest coverage TP_1 calculated for P_1 at t_0 in the reference LVLH frame are shown in Fig. 23a by the blue dotted lines and the red solid line, respectively. Meanwhile, Fig. 23b portrays the geodetic coordinates of all I_2 and TP_1 on the UTRRDE. Similarly, the intersections and the largest coverage for P_2 , P_3 , and P_4 at t_0 are portrayed in Fig. 24, Fig. 25, and Fig. 26, respectively. As shown in these figures, the results of the largest coverage coincide with the conclusion obtained in Sec. IIIB. As a result, the EZ at t_0 is ultimately obtained through Eq. (27). The geodetic coordinates of the EZ at t_0 are shown by the grey area in Fig. 27. Obviously, the EZ is equal to the remaining area after removing all the calculated largest coverage of pursuers from the entire UTRRDE. In the above simulations, the number of polygon vertices to replace I_2 was set to 360 with a step of 1° for the rotation angle α , and the time step for discrete calculations was set to approximately 5.562 s corresponding to the intersection time interval equally

divided into 200 segments, which is preliminarily determined by the intersection time range of two RRDSs. Under such parameter configurations, the computing time for a data table is about 10.934 s on an Intel(R) Core(TM) i7-7700 on a 3.60 GHz CPU.


 Fig. 27 The geodetic coordinates of EZ at t_0 on UTRRDE.

As for the two-sided optimal strategies, considering that the EZ exists at t_0 , the optimal evasion impulse is desired to achieve the largest minimum miss distance M_{\min} of all pursuers. According to Sec. IVA, the maximum M_{\min} is obtained as 1.596692 km when the longitude of the terminal evasion position r_d on UTRRDE is -3.376190° and the latitude is 37.528571° . Correspondingly, Fig. 28 illustrates the heat map of M_{\min} calculated for all the terminal evasion positions generated by traversing the longitude $\in [-180^\circ, 180^\circ]$ and latitude $\in [-90^\circ, 90^\circ]$ with the step of 1° . The maximum M_{\min} calculated is 1.576265 km when longitude = -3° and latitude = 38° , which is close to the optimization results.


 Fig. 28 Heat map of M_{\min} calculated for different r_d on EZ.

For case 2, the evasion trajectory of evader and the pursuit trajectories of pursuers are portrayed in Fig. 29 to Fig. 32. Figure 33 portrays the time history of the distance between each pursuing spacecraft and the evading spacecraft. As shown in the figures, the evading spacecraft successfully escape from all the pursuing spacecraft at 14353.583 s, which is smaller than 15715.374 s in case 1. In addition, as seen in Fig. 33, the minimum distance between pursuers and evader during the entire evasion process is 13.020359 km in case 2, which is larger than that of 6.462936 km in case 1. This is intuitive and can be accounted for by the non-optimality of the pursuing

strategy in case 2, since the pursuers did not consider any possible maneuver of the evader in this case.

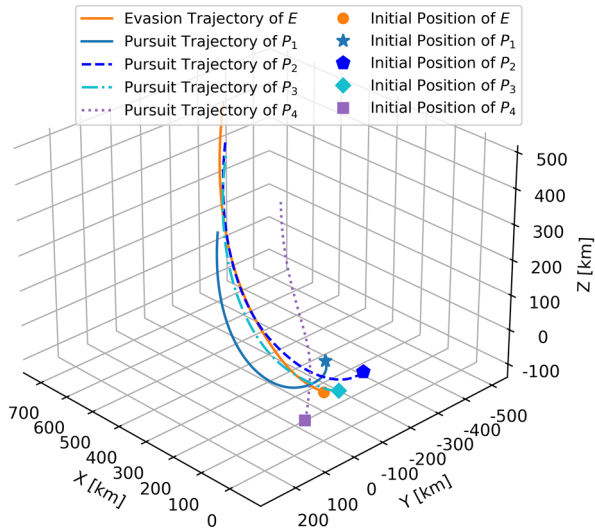


Fig. 29 The evasion and pursuit trajectories in case 2.

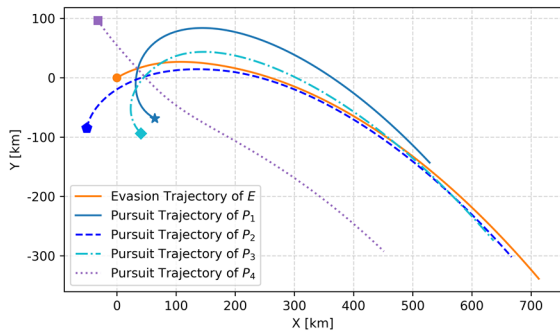


Fig. 30 The X-Y projection of transfer trajectories in case 2.

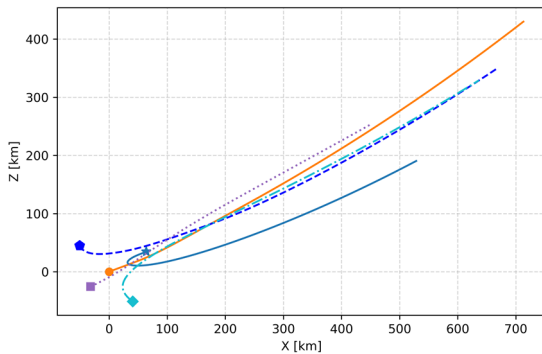


Fig. 31 The X-Z projection of transfer trajectories in case 2.

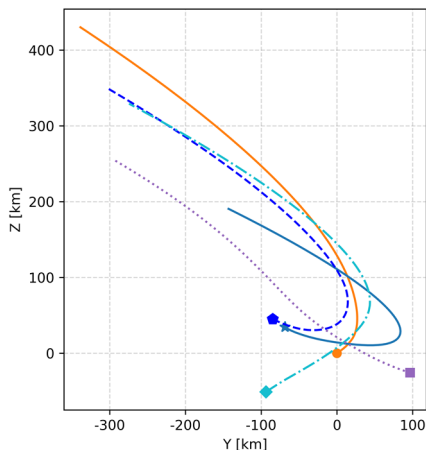


Fig. 32 The Y-Z projection of transfer trajectories in case 2.

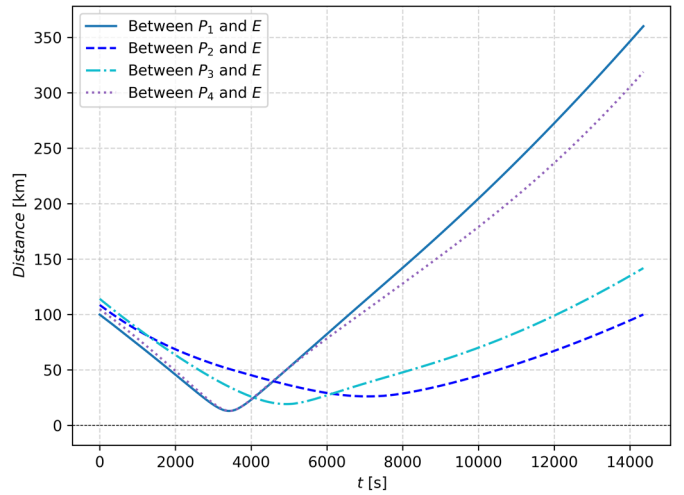


Fig. 33 Distance history between each P and E in case 2.

It should be noted that although the total time of the evasion process is relatively larger than τ , the effect of guidance can still be guaranteed because the reference orbit for optimal impulse calculation is updated to the current orbit of evader at every decision moment to make sure the RRDE of evader is always located at the origin of reference frame while calculating the EZ, and the maneuver period ΔT_d is much smaller than τ .

VI. Conclusions

In this paper, an escape-zone-based optimal evasion guidance law was proposed for an evading spacecraft on near circular reference orbit against multiple pursuing spacecraft. The concept of escape zone was presented for the impulse orbital evasion problem first. A method based on the approximate relative reachable domain ellipsoid was proposed to calculate the escape zone against multiple pursuers for each maneuver moment. The escape value was defined according to the two-sided optimal strategies analysis, and eventually used as the basis for the closed-loop evasion guidance scheme.

The proposed evasion guidance scheme provides a conservative escape-value-optimal evasion strategy for the evading spacecraft by considering the optimal intercept strategies of pursuers, such that to obtain the largest minimum miss distance of all pursuers when EZ exists or the maximum time to be intercepted by pursuers when EZ is empty. Finally, the numerical examples of an orbital evasion scenario with one evader and four pursuers were provided to verify the effectiveness of the presented method for EZ calculation and the proposed guidance scheme. The simulation results showed that the evader successfully escaped from all the pursuers in both cases against the optimal and nonoptimal pursuing strategies. Moreover, a better performance of evasion process, including a larger minimum distance and a smaller evasion time, against the nonoptimal pursuing strategy was found than that against the optimal pursuing strategy.

Acknowledgment

This study was funded by the National Natural Science Foundation of China (Grant Nos. 11972077).

Appendix A. Derivation for Approximate RRD

Considering a short-distance relative motion scenario with the circular reference orbit, after time t of applying the impulse ΔV with the components $[\Delta V_x \Delta V_y \Delta V_z]$ in the reference orbital frame, the components of the relative position of the spacecraft based on CW equations satisfy

$$\begin{cases} x = [4 - 3\cos(\omega t)]x_0 + (1/\omega)\sin(\omega t)\dot{x}_0 + (2/\omega)[1 - \cos(\omega t)]\dot{y}_0 \\ \quad + (1/\omega)\sin(\omega t)\Delta V_x + (2/\omega)[1 - \cos(\omega t)]\Delta V_y \\ y = 6[-\omega t + \sin(\omega t)]x_0 + y_0 + (2/\omega)[-1 + \cos(\omega t)]\dot{x}_0 \\ \quad + (1/\omega)[-3\omega t + 4\sin(\omega t)]\dot{y}_0 \\ \quad + (2/\omega)[-1 + \cos(\omega t)]\Delta V_x + (1/\omega)[-3\omega t + 4\sin(\omega t)]\Delta V_y \\ z = \cos(\omega t)z_0 + [\sin(\omega t)/\omega]\dot{z}_0 + [\sin(\omega t)/\omega]\Delta V_z \end{cases} \quad (\text{A1})$$

where ω is the mean angular motion of the reference orbit, x_0 , y_0 , z_0 , \dot{x}_0 , \dot{y}_0 , and \dot{z}_0 are components of the initial relative position vector and relative velocity vector in the reference local-vertical, local-horizontal (LVLH) frame, $\Delta V_x = \Delta V \cos \eta_{\Delta V} \cos \xi_{\Delta V}$, $\Delta V_y = \Delta V \cos \eta_{\Delta V} \sin \xi_{\Delta V}$, $\Delta V_z = \Delta V \sin \eta_{\Delta V}$, $\xi_{\Delta V}$ and $\eta_{\Delta V}$ are two angles characterizing the direction of the initial impulse vector in the reference LVLH frame.

Move the terms related to the initial state in Eqs. (A1) and (A2) to the left side of the equations. Taking the square of both sides and adding the two equations of x and y gives

$$\begin{aligned} & (x - \{[4 - 3\cos(\omega t)]x_0 + (1/\omega)\sin(\omega t)\dot{x}_0 \\ & \quad + (2/\omega)[1 - \cos(\omega t)]\dot{y}_0\})^2 + (y - \{6[-\omega t + \sin(\omega t)]x_0 \\ & \quad + y_0 + (2/\omega)[-1 + \cos(\omega t)]\dot{x}_0 + (1/\omega)[-3\omega t + 4\sin(\omega t)]\dot{y}_0\})^2 \\ & = \left\{ \frac{\sin^2(\omega t)}{\omega^2} + \frac{4}{\omega^2}[-1 + \cos(\omega t)]^2 \right\} \Delta V_x^2 + \left\{ \frac{4}{\omega^2}[-1 + \cos(\omega t)]^2 \right. \\ & \quad + [-3t + (4/\omega)\sin(\omega t)]^2 \left. \right\} \Delta V_y^2 + \left\{ (4/\omega^2)\sin(\omega t)[1 - \cos(\omega t)] \right. \\ & \quad \left. + (4/\omega)[-1 + \cos(\omega t)][-3t + (4/\omega)\sin(\omega t)] \right\} \Delta V_x \Delta V_y \end{aligned} \quad (\text{A3})$$

$$(z - \{\cos(\omega t)z_0 + [\sin(\omega t)/\omega]\dot{z}_0\})^2 = [\sin^2(\omega t)/\omega^2] \Delta V_z^2 \quad (\text{A4})$$

Let

$$\begin{cases} x_c = [4 - 3\cos(\omega t)]x_0 + (1/\omega)\sin(\omega t)\dot{x}_0 \\ \quad + (2/\omega)[1 - \cos(\omega t)]\dot{y}_0 \\ y_c = 6[-\omega t + \sin(\omega t)]x_0 + y_0 + (2/\omega)[-1 + \cos(\omega t)]\dot{x}_0 \\ \quad + (1/\omega)[-3\omega t + 4\sin(\omega t)]\dot{y}_0 \\ z_c = \cos(\omega t)z_0 + (1/\omega)\sin(\omega t)\dot{z}_0 \end{cases} \quad (\text{A5})$$

$$\begin{cases} \kappa_1 = \sin^2(\omega t)/\omega^2, \quad \kappa_2 = (4/\omega^2)[-1 + \cos(\omega t)]^2 \\ \kappa_3 = [-3t + (4/\omega)\sin(\omega t)]^2 \\ \kappa_4 = (4/\omega^2)\sin(\omega t)[1 - \cos(\omega t)] \\ \kappa_5 = (4/\omega)[-1 + \cos(\omega t)][-3t + (4/\omega)\sin(\omega t)] \\ \kappa_z = \sin(\omega t)/\omega \end{cases} \quad (\text{A6})$$

Then, Eqs. (A3) and (A4) can be respectively written as

$$(x - x_c)^2 + (y - y_c)^2 \leq (\kappa_1 + \kappa_2)\Delta V_x^2 + (\kappa_2 + \kappa_3)\Delta V_y^2 + (\kappa_4 + \kappa_5)\Delta V_x \Delta V_y \quad (\text{A7})$$

$$(z - z_c)^2 \leq \kappa_z^2 \Delta V_z^2 \quad (\text{A8})$$

Equations (A7) and (A8), i.e. Eq. (1) in Sec. IIA, are the calculation formulas for the three-dimensional RRD at time t . Let $F_1(t)$ denote the right side of Eq. (A7). When the relative motion time t is much smaller than the period T_r of the reference orbit, use $F_2(t) = [\kappa_2 + (\kappa_1 + \kappa_3 + \kappa_4 + \kappa_5)/2][\Delta V$

$\cos \eta_{\Delta V}]^2$ to approximate $F_1(t)$. In this way, the approximate envelope of the RRD can be obtained as

$$\frac{(x - x_c)^2}{(\kappa_{xy}\Delta V)^2} + \frac{(y - y_c)^2}{(\kappa_{xy}\Delta V)^2} + \frac{(z - z_c)^2}{(\kappa_z\Delta V)^2} = \cos^2 \eta_{\Delta V} + \sin^2 \eta_{\Delta V} = 1 \quad (\text{A9})$$

where $\kappa_{xy} = \sqrt{\kappa_2 + (\kappa_1 + \kappa_3 + \kappa_4 + \kappa_5)/2}$.

The rationality of the above approximate process is proved from the following two aspects. Firstly, the equivalence of $F_1(t)$ and $F_2(t)$ in the neighborhood of $t = 0$ for the above approximation process is demonstrated as follows:

From the specific form of each coefficient in Eqs. (A6), we have $\kappa_1(0) = \kappa_2(0) = \kappa_3(0) = \kappa_4(0) = \kappa_5(0) = \kappa_{xy}(0) = 0$. Thus, $F_1(0) = F_2(0) = 0$. Meanwhile, it can be easily proved that the expressions

$$\begin{cases} \kappa_2 - (\kappa_4 + \kappa_5)/2 \geq 0 \\ \kappa_1 - \kappa_3 \geq 0 \\ \kappa_4 + \kappa_5 \geq 0 \end{cases} \quad (\text{A10})$$

are all satisfied when $0 \leq t \leq \arctan(2/3)/\omega$. Obviously, the above expressions are also satisfied under the short-term assumption.

Let $\Delta V_{xy} = \Delta V \cos \eta_{\Delta V}$ and $\delta_{abs}(t) = |F_2(t) - F_1(t)|/F_1(t)$ denote the absolute value of the relative error caused by the approximation process. Then, we have

$$\begin{aligned} \delta_{abs} & = |[\kappa_2 + (\kappa_1 + \kappa_3 + \kappa_4 + \kappa_5)/2]\Delta V_{xy}^2 - [\kappa_1 + \kappa_2]\Delta V_x^2 \\ & \quad + (\kappa_2 + \kappa_3)\Delta V_y^2 + (\kappa_4 + \kappa_5)\Delta V_x \Delta V_y| / |(\kappa_1 + \kappa_2)\Delta V_x^2 \\ & \quad + (\kappa_2 + \kappa_3)\Delta V_y^2 + (\kappa_4 + \kappa_5)\Delta V_x \Delta V_y| \\ & = |[\kappa_2 + (\kappa_1 + \kappa_3 + \kappa_4 + \kappa_5)/2]\Delta V_{xy}^2 - [\kappa_2\Delta V_{xy}^2 + \kappa_1\Delta V_x^2 \\ & \quad + \kappa_3\Delta V_y^2 + (\kappa_4 + \kappa_5)\Delta V_x \Delta V_y]| / |(\kappa_1 + \kappa_2)\Delta V_x^2 + \kappa_3\Delta V_y^2 \\ & \quad + [\kappa_2 - (\kappa_4 + \kappa_5)/2]\Delta V_{xy}^2 + (\kappa_4 + \kappa_5)/2(\Delta V_x + \Delta V_y)^2| \end{aligned} \quad (\text{A11})$$

Substituting Eqs. (A10) into Eq. (A11), under the short-term assumption, we have

$$\begin{aligned} \delta_{abs} & \leq |[(\kappa_1 + \kappa_3 + \kappa_4 + \kappa_5)/2]\Delta V_{xy}^2 - [\kappa_1\Delta V_x^2 \\ & \quad + \kappa_3\Delta V_y^2 + (\kappa_4 + \kappa_5)\Delta V_x \Delta V_y]| / |(\kappa_1 + \kappa_2)\Delta V_x^2 \\ & = \left| \left(1 - \frac{\kappa_1}{\kappa_3}\right) \frac{\Delta V_x^2}{2\Delta V_{xy}^2} + \left(\frac{\kappa_1}{\kappa_3} - 1\right) \frac{\Delta V_y^2}{2\Delta V_{xy}^2} \right. \\ & \quad \left. + \frac{\kappa_4 + \kappa_5}{2\kappa_1} \frac{(\Delta V_x - \Delta V_y)^2}{\Delta V_{xy}^2} \frac{\kappa_1}{\kappa_3} \right| \end{aligned} \quad (\text{A12})$$

According to Eq. (A12), it is necessary to discuss the value of κ_1/κ_3 and $(\kappa_4 + \kappa_5)/(2\kappa_1)$. Let $m = \omega t$, there is

$$\lim_{t \rightarrow 0} \frac{\omega t}{\sin(\omega t)} = \lim_{m \rightarrow 0} \frac{m}{\sin m} = \lim_{m \rightarrow 0} \frac{1}{\cos m} = 1 \quad (\text{A13})$$

Thus

$$\begin{aligned} \lim_{t \rightarrow 0} \frac{\kappa_1 - \kappa_3}{\kappa_1} & = \lim_{t \rightarrow 0} \frac{-9t^2 + \frac{24}{\omega}t \sin(\omega t) - \frac{15}{\omega^2} \sin^2(\omega t)}{\sin^2(\omega t)} \omega^2 \\ & = \lim_{t \rightarrow 0} \left(-9 \left[\frac{\omega t}{\sin(\omega t)} \right]^2 + 24 \frac{\omega t}{\sin(\omega t)} - 15 \right) \\ & = 0 = 1 - \lim_{t \rightarrow 0} \frac{\kappa_3}{\kappa_1} \end{aligned} \quad (\text{A14})$$

Finally, it can be obtained as

$$\lim_{t \rightarrow 0} \frac{\kappa_1}{\kappa_3} = 1 \quad (\text{A15})$$

In addition, there is

$$\begin{aligned} \lim_{t \rightarrow 0} \frac{\kappa_4 + \kappa_5}{2\kappa_1} &= \lim_{t \rightarrow 0} \frac{-6 \sin(\cot) - 6nt \cos(\cot) + 6 \sin(\cot) \cos(\cot) + 6\cot}{\sin^2(\cot)} \\ &= \lim_{m \rightarrow 0} \frac{-6 \sin m - 6m \cos m + 6 \sin m \cos m + 6m}{\sin^2 m} \\ &= \lim_{m \rightarrow 0} \frac{-12 \cos m + 6m \sin m + 6 \cos^2 m - 6 \sin^2 m + 6}{2 \sin m \cos m} \\ &= \lim_{m \rightarrow 0} \frac{18 \sin m + 6m \cos m - 24 \cos m \sin m}{2 \cos^2 m - 2 \sin^2 m} = 0 \end{aligned} \quad (\text{A16})$$

Substituting Eq. (A15) and Eq. (A16) into Eq. (A12), it can be obtained as

$$\begin{aligned} \lim_{t \rightarrow 0} \delta_{abs} &\leq \lim_{t \rightarrow 0} \left| \left(1 - \frac{\kappa_1}{\kappa_3}\right) \frac{\Delta V_x^2}{2\Delta V_{xy}^2} + \left(\frac{\kappa_1}{\kappa_3} - 1\right) \frac{\Delta V_y^2}{2\Delta V_{xy}^2} \right. \\ &\quad \left. + \frac{\kappa_4 + \kappa_5}{2\kappa_1} \frac{(\Delta V_x - \Delta V_y)^2}{\Delta V_{xy}^2} \frac{\kappa_1}{\kappa_3} \right| = 0 \end{aligned} \quad (\text{A17})$$

Therefore, the equivalence of the above approximate process when time t approaches 0 has been proved. Secondly, a quantitative analysis has been given in Sec. IIA to investigate that the approximation process is valid for how small the motion time is. In summary, the derivation of the approximate RRD formula has been completed.

Appendix B. Guidance Scheme for Pursuing Spacecraft in Simulation Case 1 of Sec. V

The guidance scheme for the pursuing spacecraft P_i in simulation case 1 of Sec. V could be implemented as follows:

- 1) Obtain the current relative state of the evading spacecraft, and calculate the state relative to evader.
- 2) Propagate the nominal relative motion from the current state to time $T/2$ using the nonlinear relative dynamic model.
- 3) Choose a small time step t_s for the RRDE propagation. Calculate λ_0 , λ_1 and judge the positional relationship between the $RRDE_{P_i}$ and $RRDE_E$ along the nominal trajectory by Eqs. (19) to (26). Determine the type (*separation*, *intersection* or *contained*) of the nominal trajectory for P_i as in Fig. 8, and record the time t_{ex1} and t_{ex2} for the *intersection* case or time t_{ex1} , t_{in1} , t_{in2} and t_{ex2} for the *contained* case.
- 4) For the *separation* case, let the largest coverage T_{P_i} be empty, and skip to step 7.
- 5) For the *intersection* or *contained* case, calculate all the intersection curves I_1 of the $RRDE_{P_i}$ and $RRDE_E$ from 0 to τ_1 with time step t_s using the method in Sec. IIIA, and project them onto the UTRRDE through Eqs. (6) to (8) to obtain the corresponding curves I_2 . Save all the curves I_2 into the database for P_i .
- 6) Calculate the union of all I_2 to obtain T_{P_i} .
- 7) Determine the optimal pursuit maneuver by searching r_{d2} and t on T_{P_i} to minimize the miss distance M_{P_i} or directly as $\Delta V_{P_i}[r_{d2}, t_{P_i}^{\min}]$.
- 8) This procedure, given by the preceding steps, is continued until the terminal conditions of the orbital game are satisfied. If R_{\min} is smaller than $R_{\text{intercept}}$, then successful interception has been attained.

References

- [1] Luo Y., Li Z., and Zhu H.. "Survey on spacecraft orbital pursuit-evasion differential games." *SCIENTIA SINICA Technologica*, 50.12(2020):1533-1545.
- [2] Kim H. D., and Kim H. J.. "Optimal collision avoidance maneuver to maintain a LEO station keeping." *IAC-10-A6.2.9*, (2010).
- [3] Wang S., and H. Schaub. "Spacecraft collision avoidance using coulomb forces with separation distance and rate feedback." *Journal of Guidance, Control, and Dynamics*, 31.3(2008):740-750.
- [4] Wang H., Li H, Tang G.. "Collision probability based optimal collision avoidance maneuver in rendezvous and docking." *Journal of Astronautics*, 29.1(2008):220~223.
- [5] Isaacs R.. "Differential Games: A Mathematical Theory with Applications to Warfare and Pursuit, Control and Optimization." New York: John Wiley and Sons, (1965).
- [6] Berkovitz L. D.. "A Variational Approach to Differential Games." *Advances in Game Theory, Annals of Mathematics Study*. Princeton: Princeton University Press, 52(1964):127-174.
- [7] Friedman A.. "Differential Games." Rhode Island: American Mathematical Society, (1974).
- [8] Anderson G. M., and Grazier V. W.. "Barrier in Pursuit-Evasion Problems between Two Low-Thrust Orbital Spacecraft." *AIAA Journal*, 14.2(1976):158-163.
- [9] Conway B. A., and Pontani M.. "Numerical Solution of the Three-Dimensional Orbital Pursuit-Evasion Game." *Journal of Guidance Control & Dynamics*, 32.2(2009):474-487.
- [10] Sun S., Zhang Q., Loxton R., et al. "Numerical Solution of a Pursuit-Evasion Differential Game Involving Two Spacecraft in Low Earth Orbit." *Journal of Industrial and Management Optimization*, 11.4(2015):1127-1147.
- [11] Li Z. , Zhu H., et al. "A Dimension-Reduction Solution of Free-Time Differential Games for Spacecraft Pursuit-Evasion." *Acta Astronautica*, 163(2019):201-210.
- [12] Jagat A., and A. J. Sinclair. "Nonlinear Control for Spacecraft Pursuit-Evasion Game Using the State-Dependent Riccati Equation Method." *IEEE Transactions on Aerospace and Electronic Systems*, 53.6(2017):3032-3042.
- [13] Zeng X., et al. "Comparison of two optimal guidance methods for the long-distance orbital pursuit-evasion game." *IEEE Transactions on Aerospace and Electronic Systems*, 57.1(2021):521-539.
- [14] Gong H., Gong S., and Li J.. "Pursuit-evasion game for satellites based on continuous thrust reachable domain." *IEEE Transactions on Aerospace and Electronic Systems*, 56.6(2020):4626-4637.
- [15] Ghosh P., and Conway B. A.. "Near-Optimal Feedback Strategies Synthesized Using a Spatial Statistical Approach." *Journal of Guidance, Control, and Dynamics*, 36.4(2013):905-919.
- [16] Hafer W. T., et al. "Sensitivity Methods Applied to Orbital Pursuit Evasion." *Journal of Guidance Control and Dynamics*, 38.6(2015):1118-1126.
- [17] Shen H., L. Casalino. "Revisit of the Three-Dimensional Orbital Pursuit-Evasion Game." *Journal of Guidance, Control, and Dynamics*, 41.8(2018):1823-1831.
- [18] Zhang C., et al. "An optimal guidance method for free-time orbital pursuit-evasion game." *Journal of Systems Engineering and Electronics*, 33.06(2022):1294-1308.

- [19] Li Z., et al. "Saddle Point of Orbital Pursuit-Evasion Game under J2-Perturbed Dynamics." *Journal of Guidance, Control, and Dynamics*, 43.9(2020):1733-1739.
- [20] Shi M., Ye D., et al. "Spacecraft orbital pursuit-evasion games with J2 perturbations and direction-constrained thrust." *Acta Astronautica*, 202(2023):139-150.
- [21] Li Z., Zhu H., Luo Y.. "An escape strategy in orbital pursuit-evasion games with incomplete information." *Science China (Technological Sciences)*, 64.03(2021):559-570.
- [22] Lin X., Zhang G.. "Analytical State Propagation for Continuous-Thrust Linear Relative Motion." *Journal of Guidance, Control, and Dynamics*, 45.10(2022):1946-1957.
- [23] V. Chandrakanth, and D. J. Scheeres. "Delta-V-Based Analysis of Spacecraft Pursuit-Evasion Games." *Journal of Guidance, Control, and Dynamics*, 44.11(2021):1961-1971.
- [24] Wen C., and P. Gurfil. "Relative reachable domain for spacecraft with initial state uncertainties." *Journal of Guidance, Control, and Dynamics*, 39.3(2016):462-473.
- [25] Wen C., Gao Y., and Shi H.. "Three-dimensional relative reachable domain with initial state uncertainty in Gaussian distribution." *Proceedings of the Institution of Mechanical Engineers, Part G: Journal of Aerospace Engineering*, 233.5(2019):1555-1570.
- [26] Clohessy W. H., and Witshire R. S., "Terminal Guidance System for Satellite Rendezvous." *Journal of the Aerospace Science*, 27.9(1960):653-658.
- [27] Kelley, Henry J., Eugene M. Cliff, and Frederick H. Lutze. "Pursuit/evasion in orbit." *Journal of the Astronautical Sciences*, 29(1981):277-288.
- [28] Zhao L., Zhang Y., Dang Z.. "PRD-MADDPG: An efficient learning-based algorithm for orbital pursuit-evasion game with impulsive maneuvers." *Advances in Space Research*, (2023), <https://doi.org/10.1016/j.asr.2023.03.014>.
- [29] Kang Y., et al. "Reverse engineering of a Hamiltonian for a three-level system via the Rodrigues' rotation formula." *Laser Physics Letters*, 14.2(2016):025201.
- [30] Abramson, Nils, Jan Boman, and Björn Bonnevier. "Plane Intersections of rotational ellipsoids." *The American Mathematical Monthly*, 113.4(2006):336-339.
- [31] Liu J., and Zhang J.. "A new maximum simplex volume method based on householder transformation for endmember extraction." *IEEE Transactions on Geoscience and Remote Sensing*, 50.1(2011):104-118.
- [32] Klein, Peter Paul. "On the ellipsoid and plane intersection equation." *Applied Mathematics*, 3.11(2012):1634-1640.
- [33] Eisen M., A. Mokhtari, and A. Ribeiro. "Decentralized quasi-Newton methods." *IEEE Transactions on Signal Processing*, 65.10(2017):2613-2628.
- [34] <http://creativecommons.org/licenses/by/4.0/>
- [35] Bertsekas, Dimitri P. "Constrained optimization and Lagrange multiplier methods." Academic press, (2014).
- [36] Gosselin, CLÉMENT M., and J. A. O. U. A. D. Sefrioui. "Polynomial solutions for the direct kinematic problem of planar three-degree-of-freedom parallel manipulators." *Fifth International Conference on Advanced Robotics' Robots in Unstructured Environments*. IEEE, (1991).
- [37] Gillissen, I. "Area Computation of a Polygon on an Ellipsoid." *Survey Review*, 32.248(1993):92-98.
- [38] Schaub H., and Junkins J.. "Analytical Mechanics of Space Systems." AIAA, Reston, V A, (2003).
- [39] Zhou S., et al. "A self-adaptive differential evolution algorithm for scheduling a single batch-processing machine with arbitrary job sizes and release times." *IEEE transactions on cybernetics*, 51.3(2019):1430-1442.



Kunpeng Zhang received the B.Eng. degree in aerospace engineering in 2017, from the Beijing Institute of Technology, Beijing, China, where he is currently working toward the Ph.D. degree in aerospace science and technology.

His current research interests include orbital pursuit-evasion and spacecraft cooperative guidance.



Yao Zhang received the Ph.D. degree from the Beihang University, Beijing, China, in 2012.

He is an associate professor at the School of Aerospace Engineering, Beijing Institute of Technology. His area of research includes spacecraft attitude control, spacecraft vibration isolation, and spacecraft on-orbit service dynamics and control.



Heng Shi is a senior engineer at China Academy of Space Technology.

His area of research includes spacecraft attitude and orbit control, autonomous navigation, space situation awareness, spacecraft on-orbit service.



Huang Huang received her Ph.D. degree from Beijing Institute of Technology, Beijing, China, in 2011. After graduation, she joined Beijing Institute of Control Engineering and became a senior engineer in 2013.

Her research interests include spacecraft intelligent control and machine learning.



Ji Ye received the B.Eng. degree in flight vehicle design and engineering in 2021, from the Beijing Institute of Technology, Beijing China, where he is currently working toward the M.D. in aerospace science and technology.

His research interests include constellation optimization design and pursuit-evasion differential game.



Hongbo Wang received the B.Eng. degree in aerospace engineering in 2019, from the Beijing Institute of Technology, Beijing, China, where he is currently working toward the Ph.D. degree in aerospace science and technology.

His current research interests include pursuit-evasion game of spacecraft and game intention recognition.